REPORT R-457 FEBRUARY, 1970 UILU-ENG 70-202

CSL COORDINATED SCIENCE LABORATORY

TUNNELING SPECTROSCOPY IN DEGENERATE p-TYPE SILICON

D.E. CULLEN
E.L. WOLF
W. DALE COMPTON

UNIVERSITY OF ILLINOIS - URBANA, ILLINOIS

"THIS DOCUMENT HAS BEEN APPROVED FOR PUBLIC RELEASE AND SALE; ITS DISTRIBUTION IS UNLIMITED"

UILU-ENG 70-202

TUNNELING SPECTROSCOPY IN DEGENERATE p-TYPE SILICON

D. E. Cullen, E. L. Wolf, and W. Dale Compton

Coordinated Science Laboratory
and
Department of Physics
University of Illinois, Urbana, Illinois

This work was supported in part by the Joint Services Electronics Program (U.S. Army, U.S. Navy, and U.S. Air Force) under Contract DAAB 07-67-C-0199; And in part by Jet Propulsion Laboratory Contract No. 952383.

Reproduction in whole or in part is permitted for any purpose of the United States Government.

This document has been approved for public release and sale; its distribution is unlimited.

TUNNELING SPECTROSCOPY IN DEGENERATE p-TYPE SILICON*

D. E. Cullen[†], E. L. Wolf[††], and W. Dale Compton

Coordinated Science Laboratory

and

Department of Physics

University of Illinois, Urbana, Illinois

ABSTRACT

Tunneling in boron doped p-type silicon metal-semiconductor (MS) and metal-insulator-semiconductor (MIS) tunnel junctions has been studied at low temperatures by measuring the derivatives, dI/dV and d^2I/dV^2, of the current-voltage characteristics as functions of applied bias voltage V. The boron impurity concentration of the silicon crystals varied from $6.5 \times 10^{18}\,cm^{-3}$ to $2.3 \times 10^{20}\,cm^{-3}$. Junctions were prepared by evaporating metal contacts onto vacuum or air cleaved silicon surfaces.

The general features of the tunneling conductance were found to be in qualitative agreement with existing theories of tunneling in semiconductors. Structure in the derivative data resulting from the interaction of tunneling electrons with silicon zone center optical phonons and boron local mode phonons has been observed. The optical phonon lineshapes in the most heavily doped MIS units are shown to compare well with the theoretical lineshapes in which modifications in the bulk semiconductor states arising from electron-optical phonon interactions in the semiconductor electrode have been included. The origin of the optical phonon and local mode phonon structure in samples of lower doping is not fully understood.

[†]Present address: United Aircraft Research Laboratories, East Hartford, Conn.

[††]Present address: Research Laboratories Eastman Kodak Co., Rochester, New York

*This work was supported in part by the Joint Services Electronics Program (U.S. Army, U.S. Navy, and U.S. Air Force) under Contract DAAB 07-67-C-0199; and in part by Jet Propulsion Laboratory Contract No. 952383.

TUNNELING SPECTROSCOPY IN DEGENERATE p-TYPE SILICON*

D. E. Cullen†, E. L. Wolf††, and W. Dale Compton

Coordinated Science Laboratory

and

Department of Physics

University of Illinois, Urbana, Illinois

I. INTRODUCTION

Tunneling in a wide variety of semiconductor systems has been studied over the past several years. A critical review of much of this work has recently been given by Duke.[1] Of particular importance to the present work are the studies that have been made of processes involving inelastic tunneling, namely electronic tunneling with the assistance of phonons.[2,3] Such processes are exemplified by a step-like increase in conductance at a bias corresponding to the energy of the participating phonon. These effects are symmetric about zero bias. In a measurement of d^2I/dV^2 (i.e. dG/dV), such effects are seen as anti-symmetric peaks.

Wolf[4] first presented data on the tunneling into p-type silicon that clearly showed symmetric peaks in d^2I/dV^2 at the energies of the zone center optical phonon. He suggested that such effects arise from a modification in the electronic dispersion relations resulting from

---

†Present address: United Aircraft Research Laboratories, East Hartford, Conn.

††Present address: Research Laboratories Eastman Kodak Co., Rochester, New York

*This work was supported in part by the Joint Services Electronic Program (U.S. Army, U.S. Navy, and U.S. Air Force) under Contract DAAB 07-67-C-0199; and in part by Jet Propulsion Laboratory Contract No. 952383.

electron-phonon interactions. Davis and Duke[5] have shown quantitatively how such modifications can affect the structure in the tunneling conductance. They have made a detailed calculation of the shapes of the lines in d^2I/dV^2 _vs_ V. that result from these many-body interactions and have compared these calculated line shapes with experimental measurements.

This article is primarily concerned with the electron-optical phonon and electron-local mode phonon interactions in degenerate p-type silicon as revealed in electron tunneling spectra. Preliminary experimental results have already been presented[4,6] as have related theoretical studies[7,8]. We present here more extensive experimental results with particular attention to the systematic changes that occur as a function of the concentration of the boron dopant.

Small conductance peaks, about 1 meV wide, and larger conductance minima, typically 5 - 10 meV wide, were observed at zero bias in the junctions of this experiment. These features are generally categorized as "zero-bias anomalies". The wider conductance minimum, which grows in size with decreasing impurity concentration, is a prominent feature of the metal-semiconductor units and will be treated in another paper.[9] The magnetic field dependence of the narrow conductance peaks has been studied by Wolf et al.[10] These are interpreted in terms of the Appelbaum theory[11] of magnetic exchange scattering across the tunneling barrier. The required magnetic moments are thought to arise from neutral acceptors localized in the depletion region.

Two factors are worth emphasizing in considering these experiments. First, the cleavage technique used in preparing the junctions insured that

the boron density is constant to within a few angstroms of the surface. The problem inherent in fabrication methods involving thermal oxidation and etching of the silicon surface have been avoided. Tests indicate that the present method provides a simple technique for preparing tunnel junctions with reproducible characteristics. Second, a superconductor was used as the metal electrode in all cases. Data are presented <u>only</u> if the junctions exhibited the structure of the superconductor for temperatures below the transition temperature of the superconductor.

II. EXPERIMENTAL CONSIDERATIONS

A. Junction Fabrication

All of the tunnel junctions whose characteristics are to be described were fabricated from p-type silicon single crystals doped with boron. One centimeter thick slices were sawed from Czochralski grown crystals with {111} orientation. Variations in resistivity over the entire slice was verified to never be more than a few percent. The boron impurity concentrations, N_a, were obtained from the room temperature resistivity vs. impurity concentration data compiled by Irvin.[12]

Briefly, junctions were formed by cutting sample bars from a 1 cm. slice, attaching an ohmic contact, cleaving the silicon bar and evaporating a metal electrode onto the cleavage plane. Electrical contact was then made to the evaporated metal electrode. In all cases, the junctions were formed on {111} crystallographic planes.

Most of the data was obtained with junctions fabricated according to what shall be called the "dot" technique. Rectangular bars, measuring 2 x 4 x 10 mm were sawed from the silicon slices with the $\langle 111 \rangle$ axis along the 10 mm direction. All surfaces of the bars were then nickel plated using an electroless nickel plating process.[13] Proper cleansing and etching of the silicon bars in preparation for plating was found to be critical in obtaining low resistance electrical contacts. After 5 minutes in the plating solution, the samples were removed and a gold or copper wire was soldered to one of the 2 x 4 mm faces with Ceroseal solder thereby forming the ohmic return contact. The resistance of such

contacts, R_b, was determined by soldering contacts to either end of a bar plated only near the ends and measuring the conductance vs. bias of the two series contacts. For samples with N_a greater than $1.5 \times 10^{19} cm^{-3}$, R_b was less than 0.1 ohm. R_b was as high as 5 ohms for samples with $N_a = 6.3 \times 10^{18} cm^{-3}$. Since the conductance of the back contact was at least 100 times that of the tunnel junction itself, this undesirable feature of the nickel contacts was not considered serious.

It was desirable to have junctions with resistances greater than 50 ohms to avoid the distortions of the data accompanying lower resistance junctions (see IID), and to limit the junction resistance to a few kilohms since the available signal power depends inversely upon sample resistance. The ambient conditions under which the samples were cleaved were therefore tailored to produce junctions with resistances in this range and to guarantee that the back resistance was negligible compared to the junction resistance. For silicon with $N_a > 10^{19} cm^{-3}$ the junctions were formed by cleaving the bars in laboratory air allowing an insulating layer to grow on the cleavage plane. The exposure time varied from a few minutes to an hour.

Following the oxidation period, the samples were mounted in a diffusion pump vacuum system immediately above an evaporation mask containing an array of small circular holes. At pressures $< 10^{-5}$ Torr, lead or indium was evaporated through the mask onto the cleavage plane to a thickness of 0.5 to 1.0 microns in 2 to 4 minutes producing metal dots with areas of 0.0044 mm^2 to 0.032 mm^2, depending upon the mask used.

Samples with concentration $N_a < 1.5 \times 10^{19} cm^{-3}$ were cleaved in vacuum. This was accomplished with the use of a special cleaving device in the vacuum system.[15] Junctions that were prepared under conditions in which the metal-semiconductor interface contamination was minimized (ambient pressure $<10^{-6}$ Torr, minimal time delay between cleavage and exposure to the evaporating metal, and evaporation rates of 50 Å/sec or greater), were found to be of very low resistance, essentially short circuits. In order to fabricate samples with measurable resistances, it became necessary to increase the time delay and/or increase the pressure. Therefore, the lower doped samples, $N_a < 1.5 \times 10^{19} cm^{-3}$, were cleaved in vacuums of 10^{-6} to 10^{-5} Torr with time delays ranging from a few seconds up to 10 minutes.

Within a few minutes after removal from the vacuum system contact was made by lowering a spring loaded lead or indium tip onto one of the dots. The tip was fashioned by cutting a short length of 1/16 inch diameter indium or lead wire to a point using a freshly cleaned razor blade mounted in a microtome. A cold weld was formed between the tip and the dot giving the assembled system some mechanical stability. Contact forces were measured to be between 10 and 100 mg. Delays in making the contact, particularly in high humidity, allowed an oxide layer to form and prevented the formation of the cold weld.

These dot junctions, while possessing some mechanical stability, were quite delicate and great care was required when transferring the assembled junction to the liquid helium dewar. Junctions of greater mechanical stability were made by utilizing photoresist methods in making

contact to the evaporated metal dots.[16] The initial steps of this process were identical to those of the dot junction process.

After the metal dots had been evaporated onto the cleaved surface of the silicon bar and the sample removed from the vacuum system, the surface was coated with a thin layer of photoresist. The cleavage surface was then examined under a microscope and several dots located on areas free of fracture lines were selected and the areas above these dots exposed to UV light. The photoresist was then developed, producing holes thru to the original lead dots and more lead was now evaporated onto areas above the holes in the photoresist. This second layer of lead was several microns thick and about 0.5 mm x 1 mm in area. Contact to the second lead layer was then made by pressure contact. The same spring loaded tip was used to contact the second lead layer, the difference being that, this time, the tip was located at a point off the dot and more pressure was applied. The resulting system proved to be quite stable and it was possible to cycle the junctions between helium temperatures and room temperature repeatedly over an extended period of time without altering the tunneling characteristics. Unfortunately this process was developed only after most of the data on air cleaved samples had been accumulated. Nearly all of the vacuum cleaved samples were fabricated with this dot-photoresist technique.

The dot-photoresist junctions also proved valuable in establishing that the tip used in making contact to the dot samples did not damage the silicon surface and thereby influence the observed phonon lineshapes. Data obtained from dot and dot-photoresist samples are in complete agreement with one another, indicating that no such effect is occurring.

Table I contains a listing of the samples from which data will be presented. For each sample, the type of metal contact, room temperature resistivity and corresponding boron impurity concentrations are given. The method of construction, i.e., dot or dot-photoresist, is also indicated in the table. For the vacuum cleaved units, the conditions under which the unit was fabricated, namely ambient pressure and delay time, are also given. Also indicated in Table I are the calculated values of the Fermi degeneracy μ_F obtained by assuming parabolic valence bands and effective masses of $m_\ell = 0.16$, $m_h = 0.49$ and $m_{so} = 0.245$. Contributions to the density of state arising from the spin-orbit split-off band were included for values of μ_F equal to or greater than the spin-orbit splitting energy of 44 meV.[17] Although the Fermi energies thus calculated will be somewhat in error, particularly for the higher values of μ_F, these values will be sufficient for the present purpose.

In all, the authors measured over 300 junctions. The data from every sample listed in Table I was quite reproducable and every feature of the data discussed in the text was reproduced with several different junctions.

B. The Tunneling Barrier

In the case of air cleaved samples, the tunneling barrier consists of both the Schottky depletion region in the semiconductor and the oxide layer grown on the surface before evaporation of the metal contact. Because of its complexity, a precise parameterization of the barrier is not feasible. Optical measurements[18] of oxide growth on etched silicon

surfaces in room air indicate that thicknesses of about 12 Å are formed in 2 minutes and that in 3 hours this thickness has increased to about 18 Å. The thickness of the oxide film is therefore assumed to be roughly 10 to 20 Å. Metal-silicon dioxide barrier heights have been measured by Deal, Snow and Mead[19] for several metals; unfortunately neither lead nor indium were studied. The correlation between the electronegativity of the metals and the barrier height suggests, however, that for lead or indium the metal-silicon dioxide barrier is approximately 3.7 eV.

Conductivity measurements[20] on cleaved {111} silicon surfaces indicate that surface states of high density are formed at an energy of 0.60 ev ± 0.15 ev above the valence band when oxygen is absorbed on the cleaved surface. The width d_s of the Schottky depletion layer can be estimated from

$$d_s = (\varepsilon\phi_s/2\pi e N_a)^{\frac{1}{2}} \qquad (1)$$

where $\phi_s = 0.60$ eV + μ_F and N_a is the acceptor concentration near the surface. Barrier widths thus calculated range from about 20 Å for the silicon of highest doping to over 100 Å for the lower doped material. An estimate of the transmission probability of the oxide and Schottky barriers can be readily obtained in the WKB approximation. Such calculations indicate that for $N_a = 2.3 \times 10^{20}$ cm^{-3} the Schottky barrier contributes negligibly to the junction resistance while at $N_a = 2.0 \times 10^{19}$ cm^{-3} the transmission probabilities of the oxide and Schottky barriers are of comparable magnitude.

For vacuum cleaved samples the barrier configuration is less certain. Most of these junctions were prepared under conditions that

TABLE I

SAMPLE CHARACTERISTICS

N_a (cm^{-3})	Resistivity (ohm cm)	μ_F (meV)	Sample Number	Metal Electrode	Fabrication Technique	Cleavage Conditions: Vacuum (Torr x 10^6)	Cleavage Conditions: Time Delay (sec)
2.3×10^{20}	0.00054	210	57-2	In	dot	air cleaved	
			88	Pb	dot-photo	air cleaved	
1.2×10^{20}	0.0010	140	75	In	dot	air cleaved	
4.6×10^{19}	0.0026	77	81-5	In	dot	air cleaved	
2.0×10^{19}	0.0058	48	82	In	dot	air cleaved	
1.8×10^{19}	0.0065	45	127-2	Pb	dot-photo	8	600
1.35×10^{19}	0.0084	37	123-2	Pb	dot-photo	10	300
1.25×10^{19}	0.0090	35	117-1	Pb	dot-photo	6	300
9.3×10^{18}	0.0117	29	116-1	Pb	dot-photo	8	300
6.3×10^{18}	0.0162	23	113-2	Pb	dot-photo	5	15

allowed some contamination of the semiconductor surface prior to the evaporation of the metal contacts. If a sticking coefficient of unity is assumed, then at a pressure of 10^{-6} Torr, a monolayer is adsorbed in a few seconds. However, the work of Archer[18] indicates that only about 12 Å or about 3 monolayers of oxygen are adsorbed on a silicon surface in 2 minutes at atmospheric pressure. It therefore seems probable that the vacuum cleaved silicon surfaces have adsorbed no more than a single monolayer. Even so, these units cannot be described as intimate metal-semiconductor contacts of the type studied by Steinrisser et.al.[21] They can, nonetheless, be categorized as MS junctions rather than MIS junctions.

C. Sample Holders and Cryostat

Dot samples were mounted in one of two special holders designed for these units. A means of adjusting the position of the sample was provided for locating a selected dot on the sample cleavage plane under the spring loaded tip. In one sample holder the tip was pivoted from a small jewel mounted axle that was spring loaded with a watchspring. A calibrated germanium resistance thermometer was mounted close to the sample providing accurate temperature sensing. The other system, employed a thin cantilevered strip of beryllium copper spring material to provide the spring loading.[22] The indium or lead tip was soldered to the end of the beryllium copper strip.

The sample holder was then attached to the end of a stainless steel tube and immersed directly in the liquid helium. An electromagnet

capable of producing fields up to 5 kG was used for magnetic field measurements.

D. Measuring System

The ac tunneling conductance, dI/dV, and its derivative, d^2I/dV^2, were measured with the system shown in Fig. 1. Derivative techniques are familiar and only a brief description of the measuring circuit is necessary. A 400 Hz signal was applied to the series combination of the tunnel junction and a measuring resistor, R_m. The modulation was stabilized to better than 1% by the shunt resistor R_{sh}. The ac voltages developed across R_m by the ac current I(f) and the first harmonic current I(2f) were synchronously detected by a lock-in amplifier and plotted on an X-Y recorder as a function of applied dc bias voltage V. An integrator circuit was used to drive the power amplifier supplying the bias voltage. Sweep rates as low as 0.001mV/sec were attainable.

The ac currents I(f) and I(2f) at a dc bias V are given by[3]

$$I(f) = \left(\frac{dI}{dV}\right) \left[1 + \left(\frac{dI}{dV}\right) R\right]^{-1} \Delta + \text{constant} \left(\frac{d^3I}{dV^3}\right) \Delta^3 + \ldots \qquad (2)$$

$$I(2f) = 1/4\left(\frac{d^2I}{dV^2}\right) \left[1 + \left(\frac{dI}{dV}\right) R\right]^{-3} \Delta^2 + \text{constant} \left(\frac{d^4I}{dV^4}\right) \Delta^4 + \ldots \qquad (3)$$

where Δ is the peak value of the ac modulation across R_{sh}, and R is the sum of all resistances in series with the tunnel junction. Included in R, in addition to R_m, are the lead resistance, R_ℓ, back contact resistance, R_b, and the spreading resistance, R_{sp}, of the small metal dot on the silicon surface.[23] The effect of higher derivatives was minimized by reducing

the modulating voltage to the smallest value compatible with the signal-to-noise-ratio of the particular junction being studied. For dI/dV measurements this value ranged between 100 μV and 1 mV peak-to-peak, and for d^2I/dV^2 measurements the modulation voltage varied between 1 and 4 mV peak-to-peak. The term $\left[1 + (\frac{dI}{dV})R\right]$ was made as close to unity as possible by minimizing R and controlling the junction fabrication process so as to yield junctions with resistances greater than 50 ohms. R_m was usually 1 ohm and the lead resistance was about 0.5 ohm so that $R < 2$ ohm. (The back contact resistance and spreading resistance together amounted to less than 0.25 ohm for MIS units.) Thus, for a sample with an incremental resistance of 50 ohms at some value of bias V_o, the deviations from the true conductance and its derivative introduced by this factor at V_o was 4% for conductance measurements and 10% for second harmonic measurements. In most cases the sample resistance was greater than 50 ohms and the resulting deviations even smaller. This accuracy was deemed sufficient for the present purpose. Also, the position of peaks in d^2I/dV^2 is not affected by errors due to higher order terms in Eq. 3 since these terms will have even symmetry about such peaks and thus will not shift the position of these structures.

It is also important to note that the phonon lineshapes would not be noticeably altered by the corrections since the correction factor varies as $\left[1 + (dI/dV)R\right]^{-3}$, where (dI/dV)R is small (typically less than 0.04), and the change in dI/dV itself over the bias range of the phonon structure is small.

III. EXPERIMENTAL RESULTS

A. General Remarks

Figures illustrating experimental data were prepared directly from X-Y recorder plots. Tracings were made of the recorder plots and these tracings were then photographically reproduced. Since the measuring system yields I(f) and I(2f), it is acutally these quantities that appear in the figures. While the true derivaties, dI/dV and d^2I/dV^2, could have been obtained by applying the bias dependent correction factors in Eqs. 2 and 3, these corrections have not been made. As explained in Sec. IID, the parameters of the measuring circuit were chosen to minimize these corrections, and the data are therefore presented as dI/dV and d^2I/dV^2 versus V.

Positive bias corresponds to raising the Fermi level in the metal with respect to the Fermi level in the semiconductor. Thus, for positive bias the final electron state for a tunneling transition from the metal lies in the silicon valence band. At negative bias, the process may be regarded as tunneling of electrons out of occupied states in the silicon valence band into the metal. Typically, measurements were taken in the range of bias -100 mV $< V <$ 200 mV. The conductance scales are linear; the vertical scale for d^2I/dV^2 data is also linear but of arbitrary magnitude.

Structure resulting from the superconducting energy gap of the metal electrode was observed in all MIS and MS junctions at temperatures below the critical temperature of the superconductor, T_c. In the case

of the indium, this structure appeared at 3.41^{o}K within an experimental accuracy of ±0.1^{o}K. The onset of superconductivity was not observed in lead junctions since measurements were only made at 77° and at temperatures below 4.2^{o}K. A sensitive comparison of the experimental gap structure can be made with the predictions of the BCS theory by comparing the zero bias differential conductance ratio, $(dI/dV)_s/(dI/dV)_n$, with the BCS value.[24] In some cases the correspondence was found to be quite good while other junctions showed large deviations. It was observed, however, that the features of the "good" MIS junctions; namely, phonon lineshape, background conductance, etc., showed no correlation with the absence of a detailed agreement between the experimental gap structure and BCS theory.

The phonon structure associated with the superconductivity of the metal electrode was also observed. The 4.4 meV and 8.5 meV lead phonons are clearly evident in both the dI/dV and d^2I/dV^2 data of junctions with lead electrodes. Additional lead phonon structure arising from multiple phonon processes can be observed out to about 20 meV in the d^2I/dV^2 data of these lead junctions. The indium phonon structure is much weaker but can still be observed in the d^2I/dV^2 data at about 15 meV.

Tunneling measurements were usually made with the metal electrode in the normal as well as the superconducting states. Indium units were measured at 4.2^{o}K and 1.5^{o}K. Data were taken with the lead in the normal state by applying a magnetic field of a few kilogauss. It was found that fields somewhat greater than the bulk critical field were required to quench the superconductivity, presumably because of fringing of the evaporated dots.[25]

In many cases, samples of a given doping were prepared both with lead and with indium dots. The contacting tip was usually made of the same material as the dots, but in several instances indium tips were used with lead dots. Never was there any evidence of structure in the data related to the type of metal tip, and no structure, other than that due to superconductivity, could be attributed to the metal electrode material.

b. Metal-Insulator-Semiconductor-Junctions

The tunneling characteristics of MIS junctions prepared from the four most heavily doped silicon crystals are shown in Figs. 2 through 5. The general features of the conductance versus bias data are in qualitative agreement with existing predictions for metal-insulator-degenerate semiconductor contacts. Recent calculations of the conductance of such systems by Chang[26] indicate that, for a semiconductor with a relatively small Fermi degeneracy, the minimum in the conductance should occur at the Fermi energy, and for a more heavily doped semiconductor, the minimum will occur at an energy equal to or smaller than the Fermi energy. The energies of the experimental dI/dV minima are indicated in Fig. 6 and are compared with the calculated values of μ_F. At $N_a = 2.0 \times 10^{19} cm^{-3}$, the range of values brackets μ_F. At higher doping, the energies of the experimental conductance minima fall below μ_F, the difference being exaggerated by the aforementioned errors in the calculated values of μ_F. The position of the measured conductance minima therefore conform roughly with Chang's theory. The approximately

linear portion of the dI/dV curve of the most heavily doped unit (Fig. 2) in the region eV < 60 meV is in accordance with the conductance versus bias predicted by the elastic, specular tunneling model of a MIS junction in which the barrier penetration factor is taken to be a constant.

The interaction of electrons (holes) with bulk semiconductor optical phonons of small wave vector k is observed as structure in dI/dV and d^2I/dV^2 at values of applied bias such that $eV \approx \pm h\omega_o$, where $h\omega_o$ is the silicon optical phonon energy at k = 0. Raman scattering experiments at room temperature[27] and helium temperature[28] yield a value of 64.8 eV for this energy.

The position of the positive bias d^2I/dV^2 peak has been measured to be 64.2 ± 0.4 meV for samples with $N_a = 1.2 \times 10^{20} cm^{-3}$ and $2.3 \times 10^{20} cm^{-3}$. A slight shift in the peak energy is observed with decreasing doping. At $N_a = 2.0 \times 10^{19} cm^{-3}$ the peak is located at 64.5 ± 0.4 meV. Because of the large Fermi degeneracy of the silicon, it is believed that any differences between the d^2I/dV^2 peak energies and the 64.8 meV value from Raman scattering is due to phonon dispersion.[4] The observed shift of the peak towards higher energy with decreasing N_a (and thus smaller μ_F) would seem to support this explanation.

At positive bias, the electron-optical phonon interaction results in a positive step in the conductance and a corresponding peak in d^2I/dV^2 for all four values of N_a. The percentage change in conductance has been measured to be between 9 and 17%. As would be expected, this value is largest for the $N_a = 4.6 \times 10^{19} cm^{-3}$ samples where the conductance minimum is near $\hbar\omega_o$. MIS tunnel junctions fabricated from silicon with an impurity

concentration less than $2.0 \times 10^{19} cm^{-3}$ exhibit a very weak phonon structure that is barely discernible from background noise. This extreme dependence of the phonon structure upon doping is not understood at present.

The lineshape of the optical phonon at positive bias varies little with impurity concentration. At $N_a = 2.3 \times 10^{20} cm^{-3}$ (Fig. 3) the phonon structure in d^2I/dV^2 has a shallow dip below the peak, if account is taken of the rising background. Samples from the three lower doped crystals exhibit more or less a simple peak.

The optical phonon lineshape behaves quite differently at negative bias, showing a wide variation over the impurity concentration range studied. This variation with doping is summarized in Fig. 7. In samples with the three highest doping levels the lineshape of d^2I/dV^2 at negative bias is essentially a positive peak corresponding to a decrease in conductance. Samples for which $N_a = 2.3 \times 10^{20} cm^{-3}$ exhibit a sharp negative dip precending the positive peak. This dip is also present at $N_a = 1.2 \times 10^{20} cm^{-3}$ but is less pronounced. The negative bias peak for these two highest doping levels occurs at 65.4 ± 0.5 meV and is always somewhat smaller than the peak at positive bias. The change in conductivity at negative bias is $1.4 \pm 0.5\%$ for these samples. Junctions with the next lower doping, $N_a = 4.6 \times 10^{19} cm^{-3}$, also show a positive peak in d^2I/dV^2 but now the peak has shifted to a lower energy, 64.6 ± 0.5 meV, and is followed by a shallow negative dip at higher energy. The change in conductance at negative bias for these units is quite small ($<0.5\%$). No change in conductance is seen in junctions fabricated from the silicon of lowest doping. Instead, a small change in the slope of the conductance

versus bias data is observed producing a steplike change in d^2I/dV^2 as shown in Fig. 7.

Small variations in the phonon lineshapes resulting from the superconductivity of the metal electrode are observed in all MIS units. The effects of the superconductivity on the d^2I/dV^2 phonon structure in the most heavily doped units can be seen by comparing Fig. 2 with Fig. 10. In the case of the MS units of Fig. 9, the variations in the d^2I/dV^2 phonon lineshape with the superconductivity of the metal electrode are indicated in the figure by the solid and dashed line. All measurements of phonon peak energies in this experiment were made with the metal electrode in the normal state.

Additional peaks in d^2I/dV^2 near the optical phonon energy, but well resolved from it, are associated with local mode phonons of the boron acceptor impurities. This structure is strongest in the samples with the highest boron concentration where it is observed as a positive peak in both positive and negative bias at about 80 meV. At liquid helium temperatures the d^2I/dV^2 structure appears to be a single peak but as the temperature is lowered to 1.5^oK two separate peaks are resolved in forward bias as shown in Figs. 2 and 8. The negative bias structure is not clearly separated into two peaks but the presence of more than a single peak is evident in Fig. 8. The lower energy positive bias peak is located at 77.4 ± 0.4 meV. The separation of the peaks is measured to be 2.5 ± 0.5 meV.

Infrared absorption experiments[29] on silicon crystals containing up to 1.3×10^{19} boron atoms per cm^3 demonstrate that absorption peaks at

76.9 and 79.9 meV result from localized vibrations of isolated B^{11} and B^{10}, respectively. Since the natural isotopic abundances are 80% and 20% for B^{11} and B^{10} respectively, it would be expected that the strength of the two peaks would be in the ratio of 4:1. Examination of Fig. 8 reveals that, while the strengths of the two peaks cannot be accurately ascertained, the experimental data are in rough agreement with the relative abundance ratio. The small discrepancies in energy can be attributed to the proximity of the two peaks.

Boron mode structure is also observed in samples with lower boron concentration although the strength of the structure decreases rapidly with decreasing N_a and is not visible in the MIS samples of lowest doping. In MIS samples with $N_a = 1.2 \times 10^{20} cm^{-3}$ the forward bias structure is clearly visible and is roughly half as large as in the more highly doped sample. Although the negative bias structure is quite small and in some cases barely discernible, it is clear that the negative bias peak in d^2I/dV^2 due to boron is positive. In those samples with the two highest impurity concentrations the positive bias boron structure is also visible in the conductance data. The positive bias d^2I/dV^2 boron peaks are just visible above the background noise in $N_a = 4.6 \times 10^{19} cm^{-3}$ units. This strong dependance on the boron impurity concentration together with the observation of the isotope splitting firmly establish the origin of this structure as being due to tunneling with the phonon involved arising from isolated boron atoms.

C. Metal-Semiconductor Junctions

The d^2I/dV^2 tunneling characteristics of MS junctions prepared from silicon crystals with boron impurity concentrations ranging from 6.3×10^{18} cm^{-3} to $1.8 \times 10^{19} cm^{-3}$ are shown in Fig. 9. A detailed consideration of the conductance of these junctions will be the subject of another paper and will not be discussed here. The discussion in this article will be confined to the phonon structure.

The optical phonon structure, which was very weak in MIS junctions with $Na < 2.0 \times 10^{19} cm^{-3}$, is readily detected in MS junctions fabricated from the same silicon crystals. At positive bias, the optical phonon d^2I/dV^2 peak is seen in all MS units. In $N_a = 6.3 \times 10^{18} cm^{-3}$ units, the structure is weak but nevertheless detectable above the d^2I/dV^2 background. If the metal electrode is made superconducting, the peak is sharpened and more readily observed. The increase in conductance at the optical phonon energy varies from about 5% in $N_a = 1.8 \times 10^{19} cm^{-3}$ units to less than 1% in the MS junctions of lowest doping. At negative bias the optical phonon structure is detected only in samples for which $N_a \geq 1.25 \times 10^{19} cm^{-3}$. The lineshape in $N_a = 1.25 \times 10^{19} cm^{-3}$ junctions is similar to that seen in $N_a = 2.0 \times 10^{19} cm^{-3}$ MIS units (Fig. 5); i.e., a step down in d^2I/dV^2 as the bias is increased in the negative direction. At $N_a = 1.8 \times 10^{19} cm^{-3}$, the negative bias optical phonon lineshape resembles that seen in $N_a = 4.6 \times 10^{19} cm^{-3}$ MIS units (Fig. 4). In all cases the negative bias optical phonon structure in MS junctions is quite weak, making clear identification of the lineshape difficult.

The boron local mode phonon structure, which was not clearly detectable in the lower doped MIS junctions, is evident in the d^2I/dV^2 data of MS junctions with $N_a \geq 9.3 \times 10^{18} cm^{-3}$. While the boron structure was not observed at negative bias in these MS units, the positive bias boron peak is seen to be much larger in comparison to the optical phonon peak than it was in the MIS samples. The d^2I/dV^2 boron peak is roughly half as large as the optical phonon peak. The effect of the superconductivity of the metal electrode on the MS phonon lineshapes is shown by the dashed lines in Fig. 9.

IV. DISCUSSION OF RESULTS

For all MIS junctions with $N_a > 2 \times 10^{19} cm^{-3}$, the interactions between tunneling electrons and optical phonons results in structure in the conductance, dI/dV, which is approximately antisymmetric about zero bias. The corresponding d^2I/dV^2 lineshapes are approximately symmetric about V=0 as seen in Figs. 2, 3, 4, and 8. This symmetry is of particular importance for it distinguishes these lineshapes from those that would result from phonon-assisted tunneling.

Davis and Duke(4) have calculated the influence of electron interactions with optical phonons on the electronic self-energies in degenerate semiconductors. They have numerically evaluated the effects of such many-body interactions on the tunneling conductance for the case of p-type silicon MIS junctions. The resulting theoretical lineshape is in qualitative agreement with the structure observed in the $N_a = 2.3 \times 10^{20} cm^{-3}$ junctions as shown in Fig. 10. Specifically, the calculated d^2I/dV^2 lineshape has the same symmetry about zero bias, the same relative size of forward to reverse bias structure, and the shape of the theoretical curve closely resembles the experimental data. The symmetric second derivative structure is therefore believed to result primarily from an electronic self-energy effect in the semiconductor electrode due to interactions of the tunneling particle and the optical phonons.

Treating the boron impurity as a harmonic oscillator in a degenerate hole (electron) fluid, Davis and Duke(5) also calculated the hole-local mode phonon coupling in silicon. They find that the form of

the coupling is essentially identical to the hole-LO-phonon coupling in a polar semiconductor. The d^2I/dV^2 lineshapes resulting from polar coupling (Fig. 8, Ref. 5) are similar to those obtained with the use of deformation potential coupling appropriate for silicon (dashed curve in Fig. 10). In both cases the phonon interaction results in a nearly symmetric second derivative structure. The symmetric nature of the experimental boron mode d^2I/dV^2 structure in the $N_a = 2.3 \times 10^{20} cm^{-3}$ units therefore suggests that this too is the result of an electron self-energy effect rather than an inelastic phonon emission process.

As the boron impurity concentration is reduced, the MIS optical phonon lineshapes show increasing deviations from the calculated self-energy lineshape of Davis and Duke.[5] These variations with doping are particularly evident at negative bias as shown in Fig. 7. Duke and Kleiman[30] have recently calculated the self-energy lineshapes for silicon of lower doping. Their results indicate that the self-energy d^2I/dV^2 lineshapes, particularly at negative bias, are not sensitive to the doping of the semiconductor. Therefore, the variations in the experimental d^2I/dV^2 structure with doping cannot be attributed to a dependence of the bulk self-energy effect upon impurity concentration.

In view of the concentration dependence of the experimental data and the recent calculation by Duke and Kleiman[30], it appears that other effects must be present. One might ask, for example, whether the data can be explained by assuming that both self energy effects and phonon assisted tunneling contribute to a significant degree, particularly in

the case of the lower doped junctions.

In $N_a = 2.0 \times 10^{19} cm^{-3}$ samples, for instance, the silicon Fermi degeneracy is about 48 meV, which is considerably less than the zone center optical phonon energy of 64.8 meV. Thus, at a positive bias equal to the phonon energy, electrons tunneling from states near the Fermi level of the metal electrode are tunneling into a state in the forbidden gap of the semiconductor. Emission of an optical phonon may allow this to occur. Self-energy effects at positive bias are expected to be weaker for those cases in which $\hbar\omega_o > \mu_F$. Since, however, there is no drastic change in the structure of the line at this dopant level, it is likely that inelastic phonon emission plays a reasonably important role in these lower doped junctions.

At negative bias, the situation is somewhat different. The negative d^2I/dV^2 peak characteristic of phonon assisted tunneling was not detected in any of the tunnel junctions of this experiment, and hence there is no evidence for this mechanism at negative bias. Structure resulting from self-energy effects at negative bias is not expected to be sensitive to whether μ_F is greater or less than $\hbar\omega_o$ as was the case at positive bias. At a negative bias equal to the phonon energy, electrons are tunneling from states deep in the silicon valence band and calculations of the self-energy effect are therefore insenstive to the degeneracy of the semiconductor.[30] The bulk self-energy effect is thus expected to be more evident at negative bias than at positive bias for material in which $\mu_F < \hbar\omega_o$.

Thus, the experimental optical phonon lineshapes in the sequence of MIS samples examined in this work cannot be satisfactorily explained either in terms of the bulk self-energy effect alone or in terms of a combination of bulk self-energy and phonon assisted tunneling. In addition, even in the most heavily doped units, where the agreement is best between the experimental d^2I/dV^2 data and the bulk self-energy lineshape calculated by Davis and Duke,[5] there is a lack of detailed agreement between theory and experiment (see Fig. 10). At positive bias, the sharp negative dip preceeding the positive peak is not observed experimentally. At negative bias, the theory predicts a substantial change in the slope of the dI/dV characteristic as the bias is swept from one side of the optical phonon structure to the other. The experimental data show no such change in slope.

Duke has pointed out that the phonon structure can be influenced by self-energy effects arising from interactions in the barrier region as well as from interactions in the bulk.[31] Such barrier self-energy effects might be expected to depend rather strongly upon impurity concentration since various properties of the barrier itself vary with doping. The dependence of the negative bias optical phonon d^2I/dV^2 lineshapes upon impurity concentration might then be explained in terms of the dependence of the barrier self-energies upon doping. In particular, it is thought that the self-energies and hence the lineshapes may be influenced by changes in the screening in the semiconductor depletion region adjacent to the bulk where the free carrier concentration in non-zero.

Brailsford and Davis[32] have recently shown that structure in the lineshapes, similar to that obtained with many-body effects, can occur due to a combination of the inelastic process involving phonon emission and interference between the elastic channel and a two-step process involving the excitation and subsequent de-excitation of electrons by phonon emission.

The features of the boron local mode phonon structure tend to support the conclusions that interactions in the barrier region and screening are important factors. The symmetry of the boron d^2I/dV^2 structure in the $N_a = 2.3 \times 10^{20} cm^{-3}$ MIS junctions was used to distinguish that structure from inelastic phonon assisted tunneling. In the lower doped units, both MS and MIS, the boron structure is not observed at negative bias and so an identification on the basis of symmetry about V=0 cannot be made. Even so, the variations in the strength of the effect with impurity concentration and method of device fabrication (MS or MIS) allow certain inferences to be drawn.

In the MIS junctions, where the impurity concentration varied between $2.0 \times 10^{19} cm^{-3}$ and $2.3 \times 10^{20} cm^{-3}$, the positive bias boron local mode phonon peak was approximately 25% as large as the optical phonon peak in the most heavily doped units and the relative size diminished with decreasing boron content until it became nearly undetectable at $N_a = 2.0 \times 10^{19} cm^{-3}$. For MIS samples with $N_a < 2 \times 10^{19} cm^{-3}$, neither the boron structure nor the silicon optical phonon structure were unambiguously detected. Both of these phonon peaks were observed in MS junctions fabricated from crystals with the same doping. In MS

units with N_a between $9.3 \times 10^{18} cm^{-3}$ and $1.8 \times 10^{19} cm^{-3}$ the boron peak was approximately 40% as large as the optical phonon peak and this proportion varied less than 10% over that range of doping. The fact that the phonons can easily be detected in MS junctions but not in MIS junctions made from the same semiconductor material is almost certainly related to the properties of the barriers. That the addition of the oxide layer should decrease the transmission of the barrier and make detection of the phonon peaks more difficult is not unexpected. However, not only does the oxide layer cause a rapid decrease in the strength of the phonon structure for silicon with $N_a < 2 \times 10^{19} cm^{-3}$; but, as is evident by comparing the data from MS and MIS junctions in this region of concentration, the optical phonon and local mode phonon structures are not equally affected by the insulating barrier. In MIS units with $N_a = 2.0 \times 10^{19} cm^{-3}$, the boron phonon peak was not clearly detected and certainly was less than 10% of the optical phonon peak. In MS units with $N_a = 1.8 \times 10^{19} cm^{-3}$, the local mode phonon peak was 40% as large as the optical phonon peak and represented an increase in conductance of approximately 2%. This change in the relative size of the boron peak with the type of barrier is indicative of the importance of the barrier in determining the phonon structure. When the oxide is present, the silicon optical phonon effect is dominant and the interaction with boron local mode phonons play a secondary role. With no oxide and a barrier consisting of only the Schottky depletion region in the silicon, the boron phonon structure becomes comparable in magnitude to the optical phonon structure. It seems unlikely that electron-phonon

interactions in the semiconductor bulk would be sensitive enough to the nature of the tunneling barrier to produce these effects.

It is concluded, on the basis of these observations, that the interactions giving rise to the optical and local mode phonon structure in the lower doped units occur primarily in the barrier region. Also, the fact that the relative size of the boron peak in the MS units remains essentially constant while the boron concentration decreases by a factor of two may suggest that screening plays an important part in determining the local mode phonon structure. The reduction in screening at lower boron concentrations presumably leads to an increase in the strength of the interaction that is large enough to conterbalance the decrease in density of boron impurity atoms.

It was noted previously that in MIS junctions with $N_a \leq 1.8 \times 10^{19} cm^{-3}$ the phonon structure was very weak. In view of the fact that the phonons were easily detected in MS units with the same doping, the rather sudden disappearance of the phonon structure in the MIS units is not fully understood. At a doping of $N_a = 1.8 \times 10^{19} cm^{-3}$, the Fermi degeneracy is about 45 meV, and thus close to the spin-orbit splitting energy of 44 meV. If tunneling into the split-off valence band is somehow more probable than tunneling into the light- and heavy-hole bands, then the fact that the phonons seem to disappear when μ_F becomes less than E_{so} may not be coincidental. More probably, the structure is simply lost in the noise, as MIS units with $N_a \leq 1.8 \times 10^{18} cm^{-3}$ tended to have higher resistances and consequently the data exhibited poorer signal-to-noise.

V. SUMMARY

The present measurements demonstrate that electron tunneling is an effective probe of the collective excitation spectra of degenerate semiconductors and of some of the properties of the tunneling barrier. The results presented here suggest that a satisfactory description of the dependence of dI/dV and d^2I/dV^2 upon V involves an understanding of the relative importance of three processes, namely, i) inelastic effects in which phonons are emitted, ii) many-body effects in the bulk of the semiconductor, and iii) many-body effects in the barrier, particularly in the Schottky barrier of the semiconductor.

At very high dopant levels, the lineshape in d^2I/dV^2 is reasonably well fitted by a theory that considers only many-body effects in the bulk semiconductor. At these dopant levels, the many-body effects may dominate. It has not been proved, however, that these lineshapes cannot also result from inelastic processes that interfere with elastic processes.

Since no discontinuity is observed in the shape of the d^2I/dV^2 peaks as the dopant level is decreased to a point where $\hbar\omega_o > \mu_F$, it is suggested that many-body bulk effects cannot dominate the processes at these doping levels. In fact, this suggests that phonon assisted processes increase in importance as the doping decreases.

At still lower doping levels, in which data on both MS and MIS junctions were obtained, the importance of interactions in the barrier becomes evident. In particular, the probability of interactions between tunneling electrons and unscreened ionized boron acceptor impurities is

greatly increased at the lower concentrations. Thus, the properties of the barrier begin to dominate and the characteristics of it must be considered.

Acknowledgments

The authors are indebted to Professor C. B. Duke and Dr. L. C. Davis for many valuable discussions of the experimental results and their interpretation. We also thank Professor N. Peacock for the use of his vacuum system.

References

1. C. B. Duke, Tunneling in Solids (Academic Press Inc., New York, 1969).

2. N. Holonyak, Jr., I. Lesk, R. Hall, J. Tiemann, and H. Ehrenreich, Phys. Rev. Letters 3, 167 (1959).

3. R. T. Payne, Phys. Rev. 139, A570 (1965).

4. E. L. Wolf, Phys. Rev. Letters 20, 204 (1968).

5. L. C. Davis and C. B. Duke, Phys. Rev. 184, 764 (1969).

6. D. E. Cullen and W. D. Compton, Bull. Am. Phys. Soc. 14, 414 (1969).

7. L. C. Davis and C. B. Duke, Solid State Comm. 6, 193 (1968).

8. L. C. Davis, Phys. Rev. (to be published).

9. D. E. Cullen, W. D. Compton and E. L. Wolf (to be published).

10. E. L. Wolf and D. L. Losee, Solid Comm. 7, 665 (1969); D. L. Losee and E. L. Wolf, Phys. Rev. Letters 23, 1457 (1969).

11. J. Appelbaum, Phys. Rev. 154, 633 (1967).

12. J. Irvin, Bell Sys. Tech. J. 41, 387 (1962).

13. M. V. Sullivan and R. M. Warner, Jr. in Transistor Technology, V. 3 (F. J. Biondi, Ed.) D. Van Nostrand Co. Inc., New York, 1958).

14. G. W. Gobeli and F. G. Allen, J. Phys. Chem. Solids 14, 23 (1960).

15. E. L. Wolf and W. D. Compton, Rev. Sci. Inst. 40, 1497 (1969).

16. The authors are indebted to Professor N. Peacock for suggesting this method and to Mr. L. Schein for assistance.

17. S. Zwerdling, K. J. Button, B. Lax and L. M. Roth, Phys. Rev. Letters 4, 173 (1960).

18. R. J. Archer, J. Electrochem. Soc. 104, 620 (1957).

19. B. E. Deal, E. H. Snow, and C. A. Mead, J. Phys. Chem. Solids 27, 1873 (1966).

References (Continued)

20. D. Aspnes, Surface Science 4, 353 (1966).

21. F. Steinrisser, L. C. Davis and C. B. Duke, Phys. Rev. 176, 912 (1968).

22. The authors are indebted to Professor N. Peacock for his assistance in designing this sample holder.

23. W. Shockley, Electrons and Holes in Semiconductors, (D. Van Nostrand Co. Inc., New York, 1950) p. 99.

24. J. Bardeen, L. Cooper and J. Schrieffer, Phys. Rev. 106, 162 (1957).

25. H. L. Caswell, J. Appl. Phys. 32,105 (1961).

26. L. L. Chang, J. Appl. Phys. 39, 1455 (1968).

27. J. H. Parker, Jr., D. W. Feldman, and M. Askin, Phys. Rev. 155, 712 (1967).

28. G. B. Wright and A. Mooradian, Phys. Rev. Letters 18, 608 (1967).

29. M. Balkanski and W. Nazarewicz, J. Phys. Chem. Solids 27, 671 (1965).

30. C. B. Duke and G. G. Kleimann (to be published in Phys. Rev.).

31. C. B. Duke (private communication).

32. A. D. Brailsford and L. C. Davis (private communication).

FIGURE CAPTIONS

Fig. 1. Simplified schematic of derivative measuring system.

Fig. 2. Tunneling characteristics of silicon MIS junction No. 88 containing $2.3 \times 10^{20} cm^{-3}$ boron impurities.

Fig. 3. Tunneling characteristics of silicon MIS junction No. 75 containing $1.2 \times 10^{20} cm^{-3}$ boron impurities.

Fig. 4. Tunneling characteristics of silicon MIS junction No. 81-5 containing $4.6 \times 10^{19} cm^{-3}$ boron impurities.

Fig. 5. Tunneling characteristics of silicon MIS junction No. 82 containing $2.0 \times 10^{19} cm^{-3}$ boron impurities.

Fig. 6. Energies of the dI/dV minima versus doping. The calculated Fermi degeneracy is shown for comparison. For each value of N_a, the range over which the experimental dI/dV minima occurred is indicated by the extent of the vertical bars. At $N_a = 4.6 \times 10^{19} cm^{-3}$, this range is unusually large due to the proximity of the optical phonon structure which tends to shift the position of the dI/dV minimum.

Fig. 7. Summary of the MIS optical phonon d^2I/dV^2 lineshapes at negative bias. The vertical scales are not necessarily the same.

Fig. 8. d^2I/dV^2 phonon lineshapes of a $N_a = 2.3 \times 10^{20} cm^{-3}$ MIS junction. The vertical scales and zeros are different for each curve. Peak-to-peak modulation = 1 mV.

FIGURE CAPTIONS (continued)

Fig. 9. d^2I/dV^2 versus V data from typical MS junctions prepared from the five lower doped crystals. The data near zero bias has been omitted and the positive and negative bias data have been displaced vertically with respect to one another for simplicity of presentation.

Fig. 10. Comparison of the calculated d^2I/dV^2 lineshape of Davis and Duke[5] with experiment. The parameters of the theoretical curve are given in Ref. 7 . Since the calculated background does not accurately depict the experimental background; it was necessary to shift the experimental negative bias phonon structure vertically to coincide with the theoretical curve.

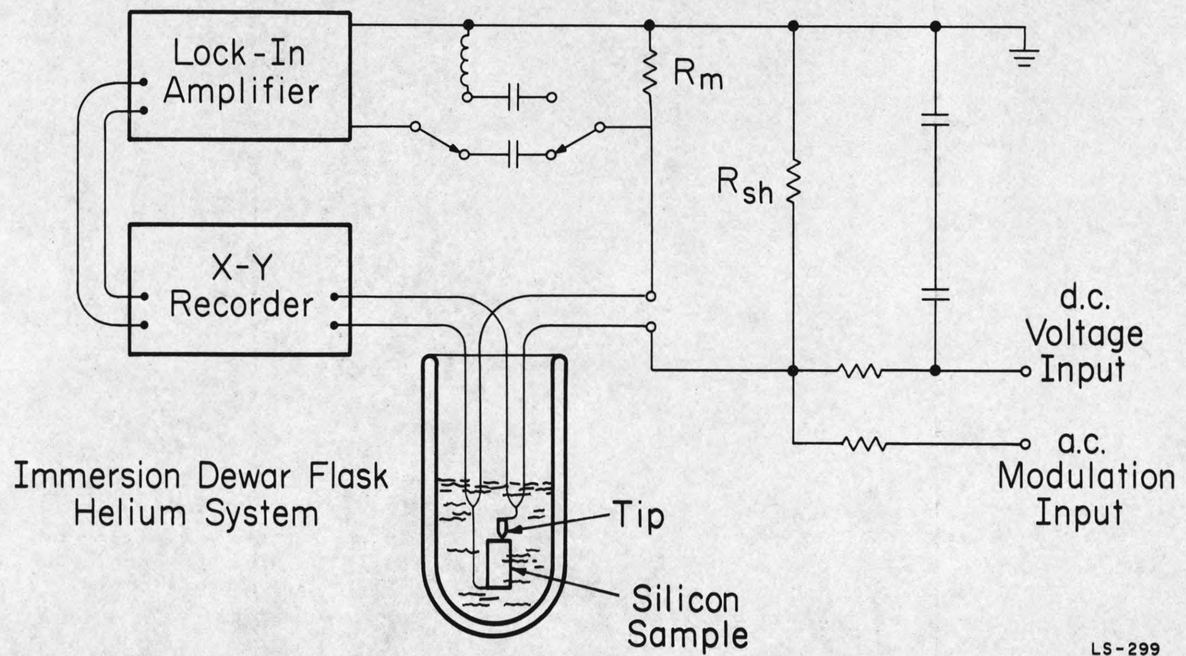

Figure 1

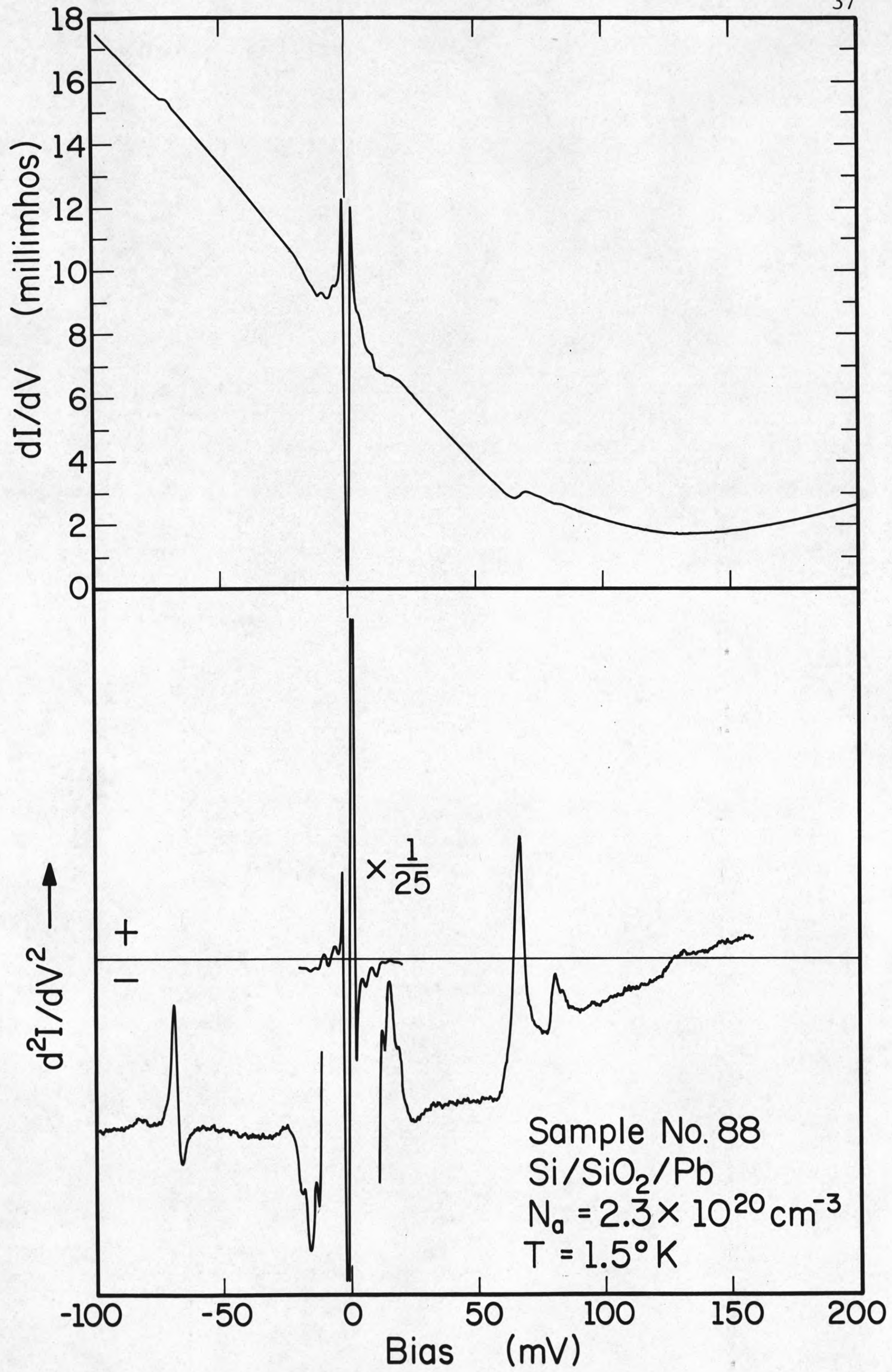

Figure 2

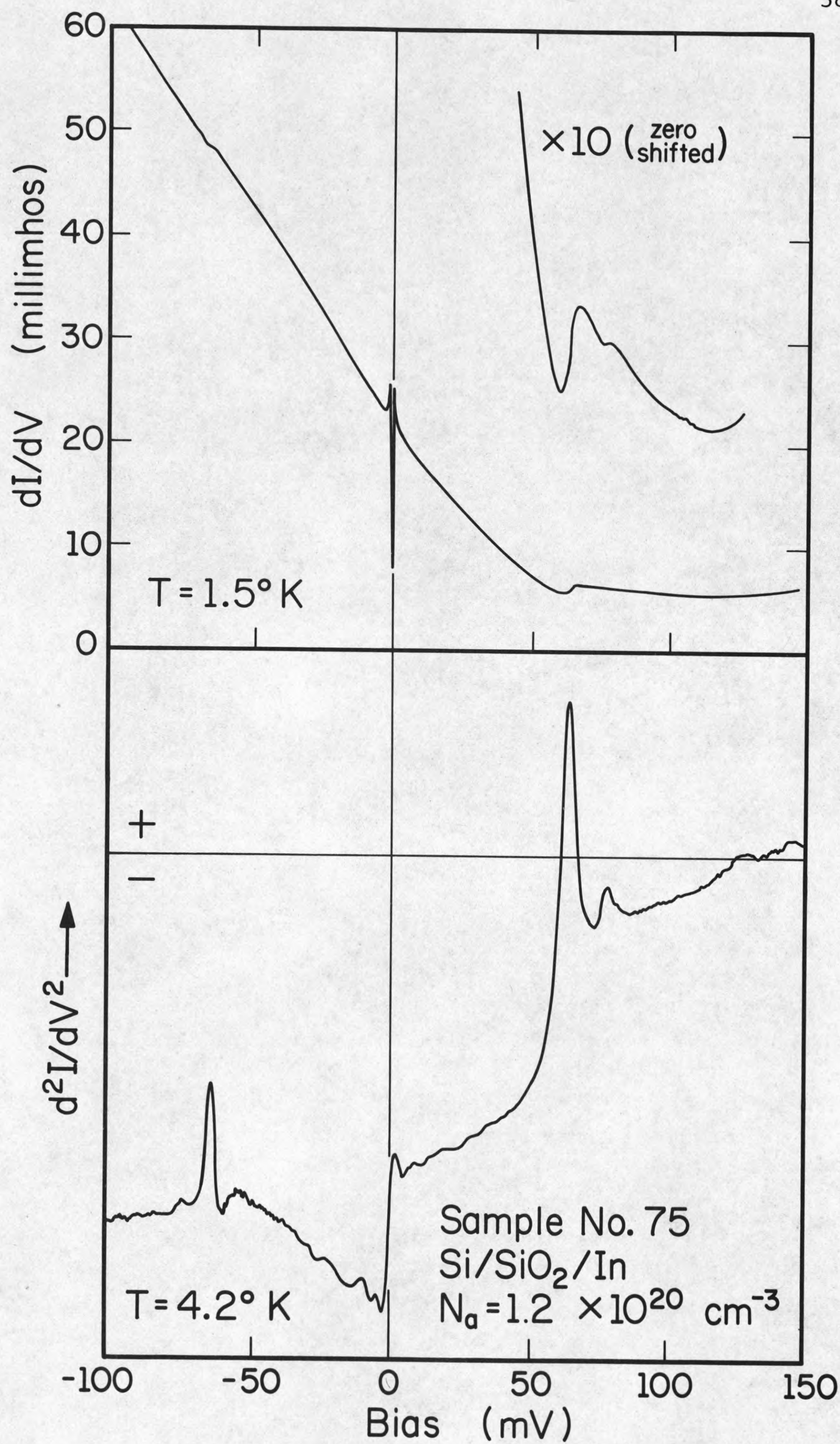

Figure 3

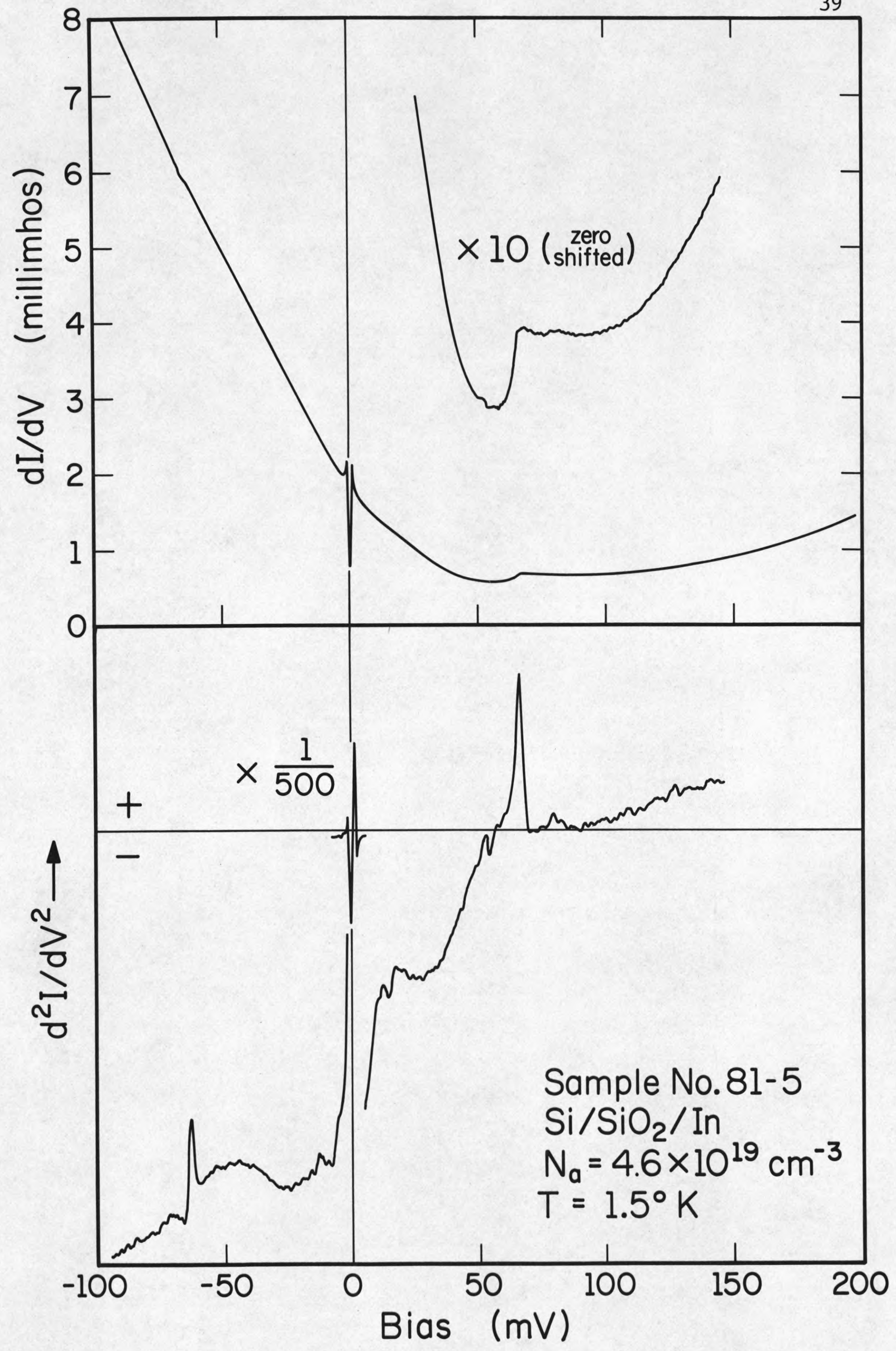

Figure 4

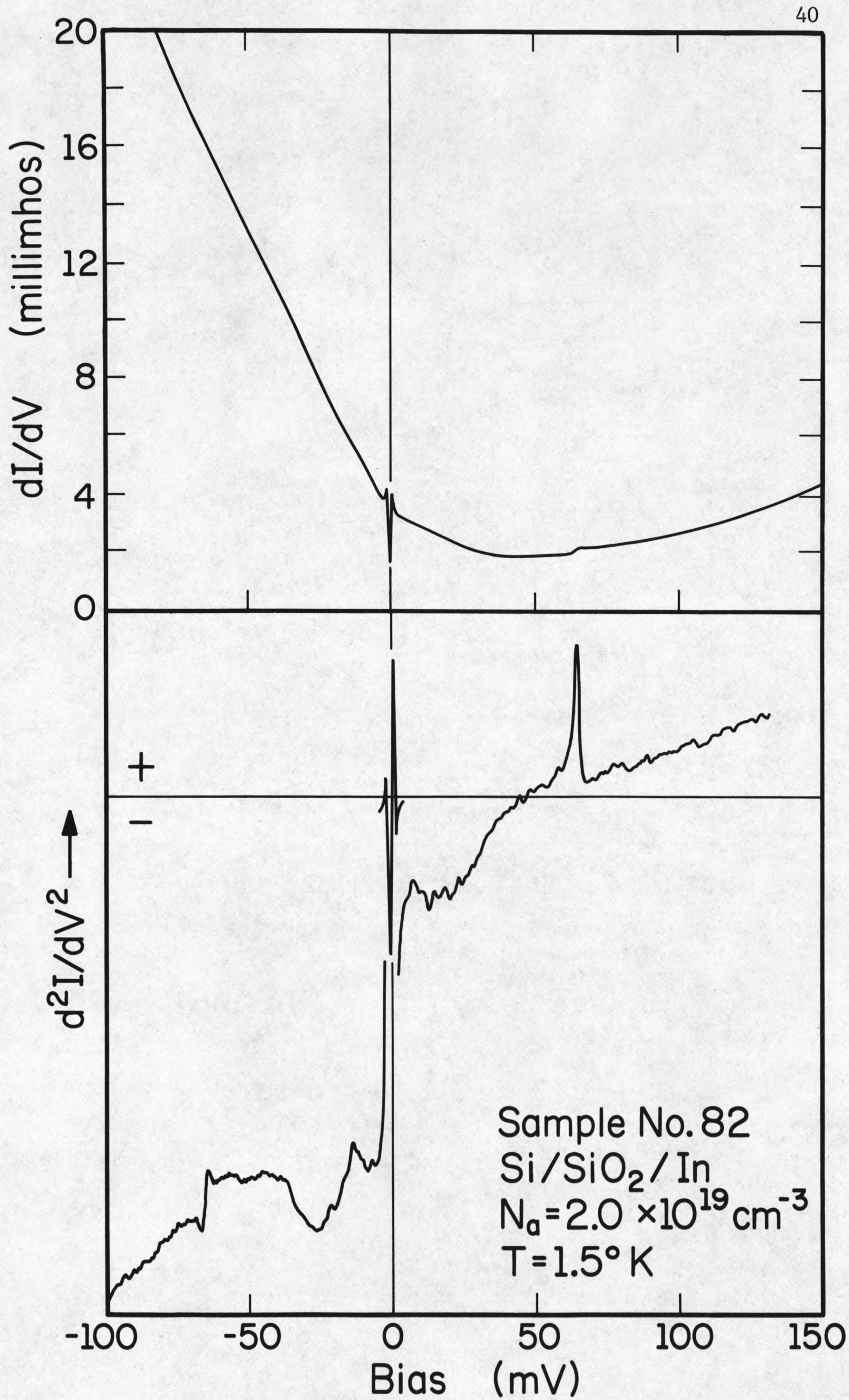

Figure 5

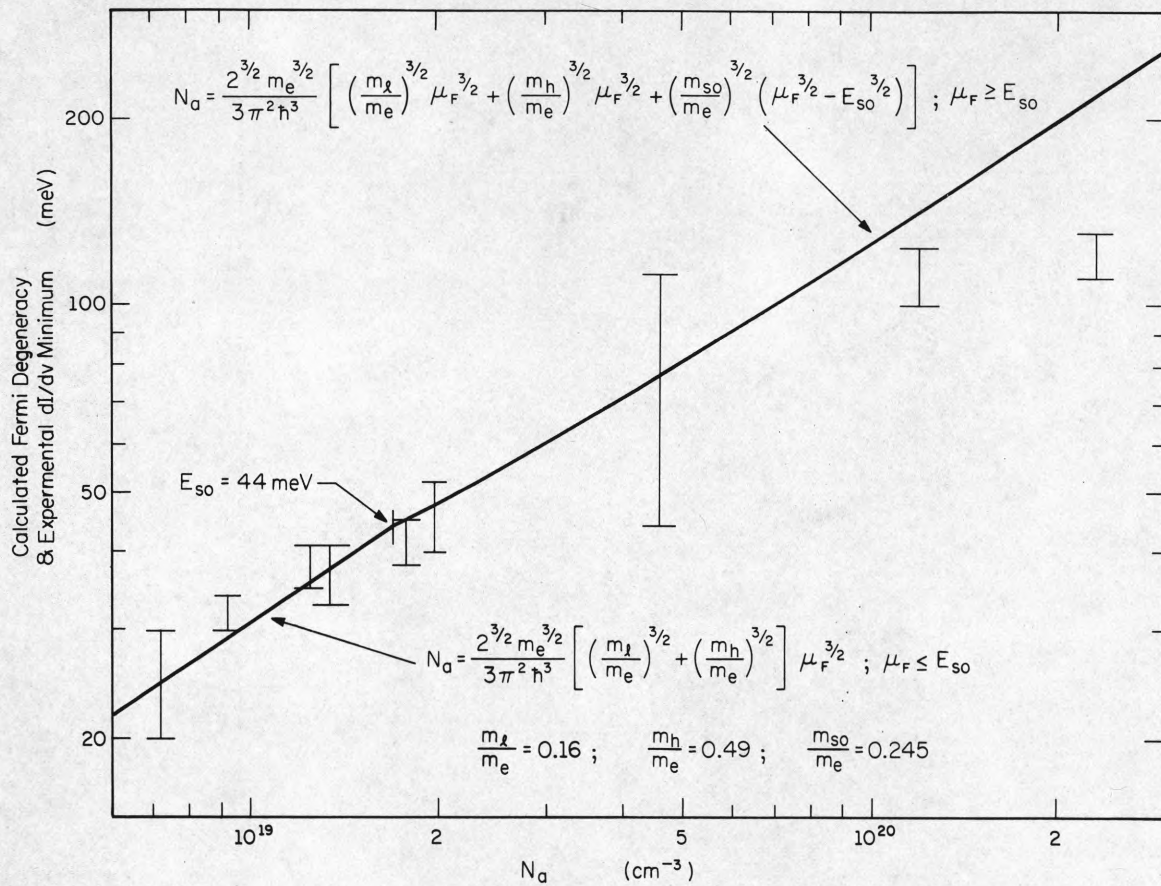

Figure 6

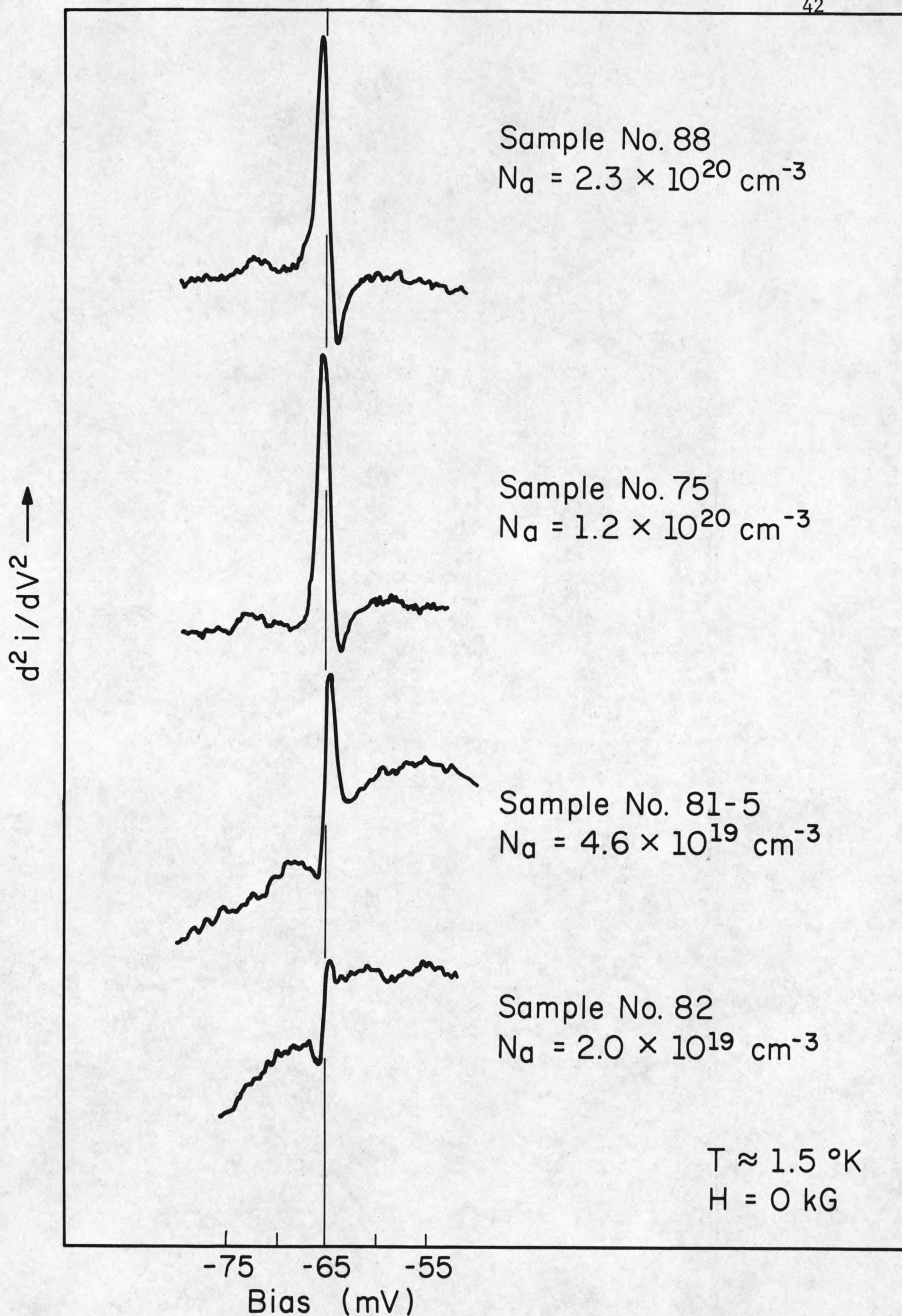

Figure 7

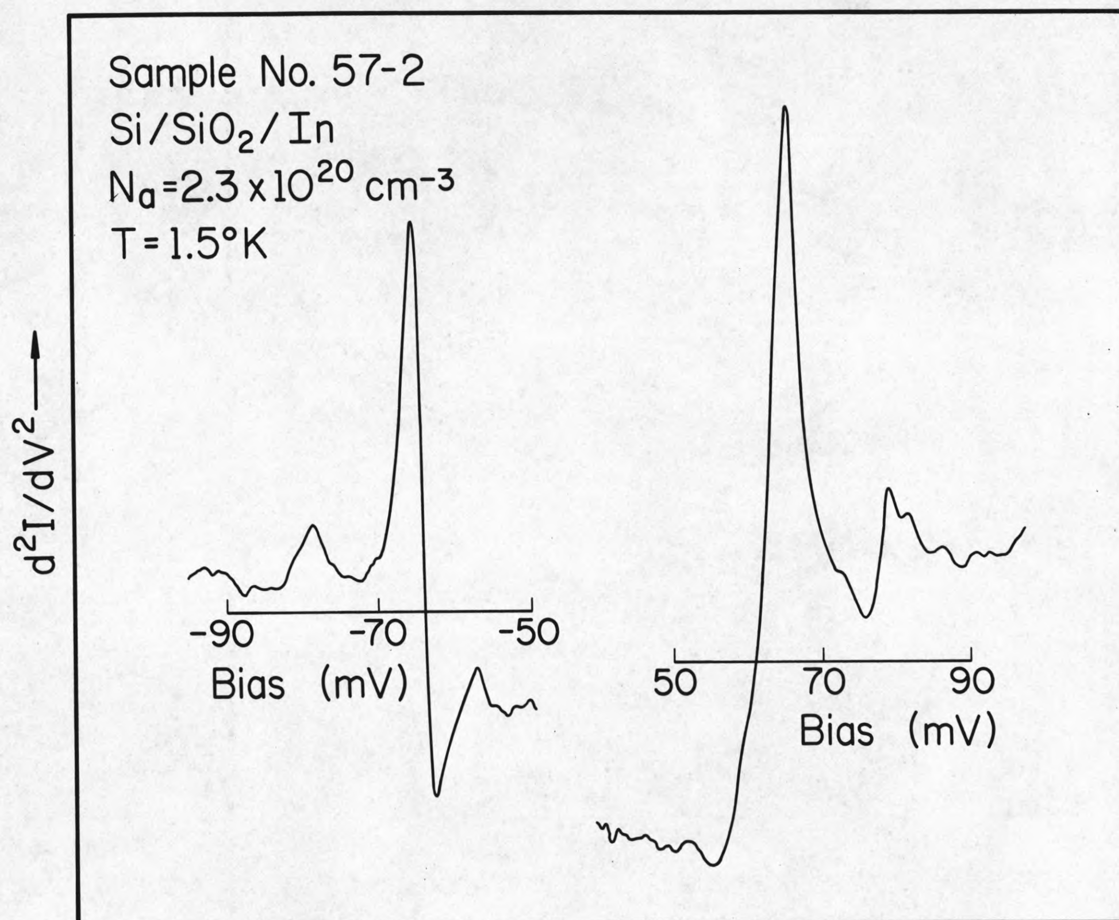

Figure 8

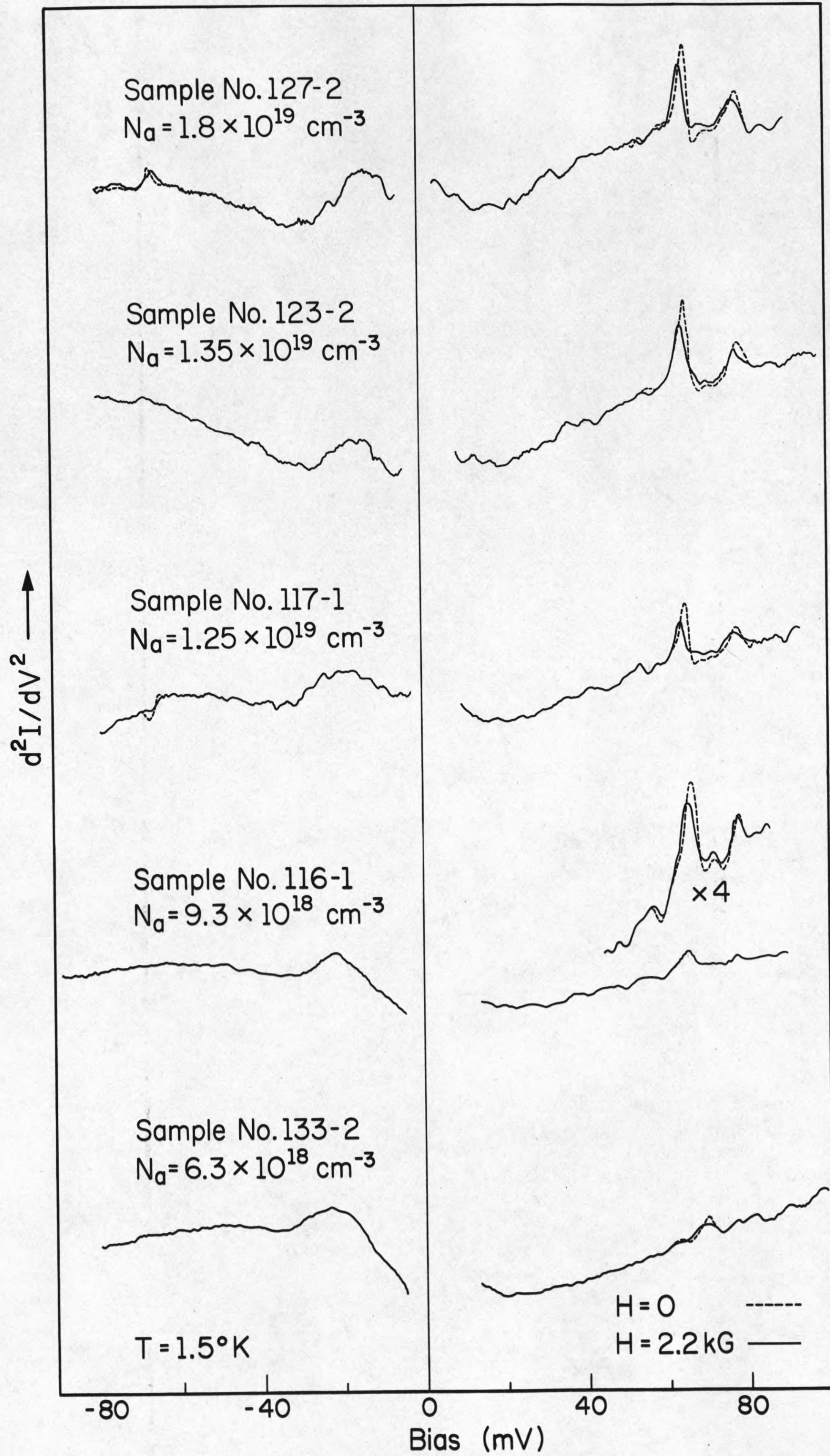

Figure 9

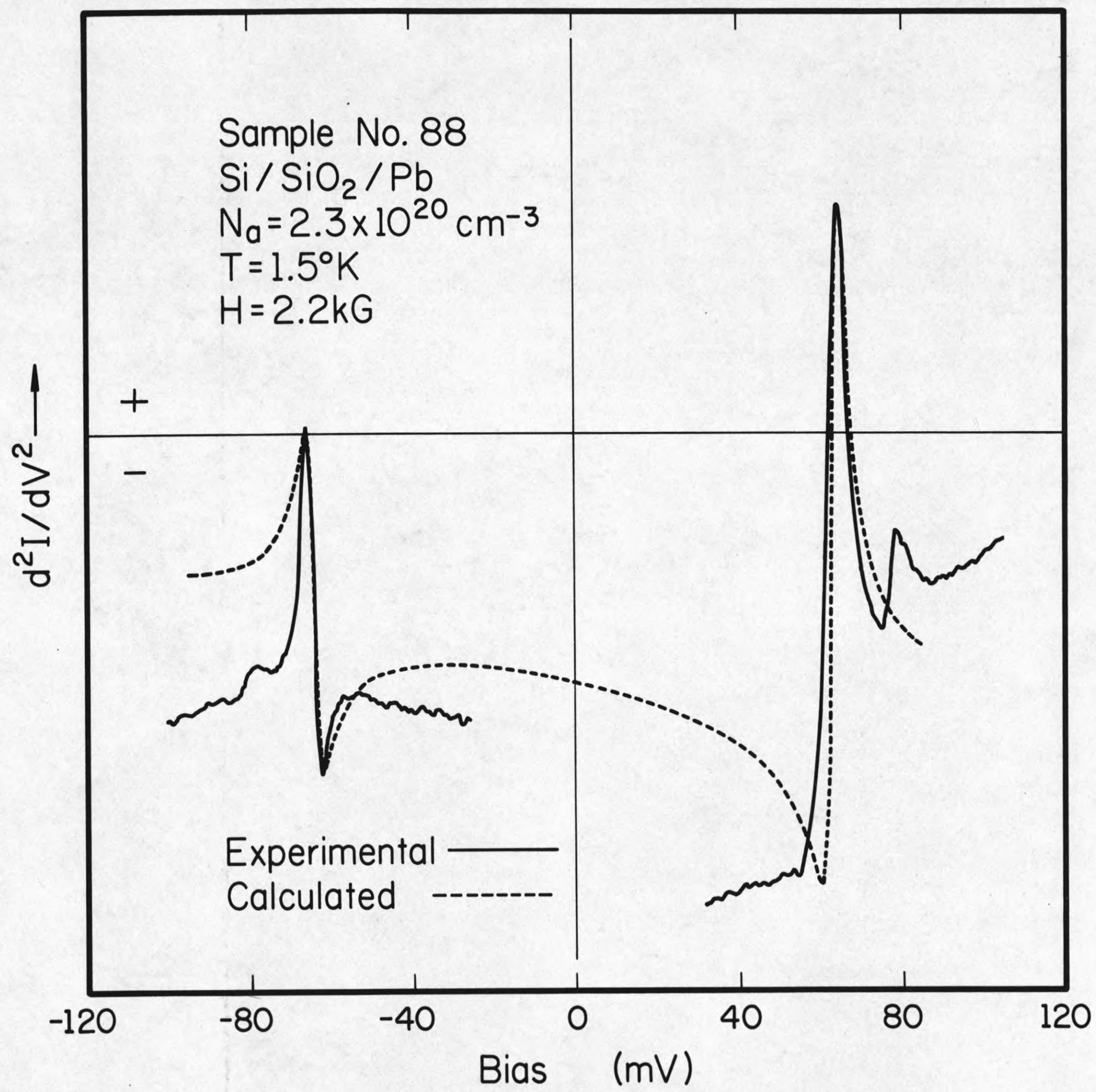

Figure 10

Distribution List as of November 1, 1969

Defense Documentation Center
Attn: DDC-TCA
Cameron Station 50 Copies
Alexandria, Virginia 22314

ESD (ESTI)
L. G. Hanscom Field
Bedford, Mass. 01731 2 Copies

Director, Electronic Programs
Attn: Code 427
Department of the Navy
Washington, D. C. 20360 3 Copies

Naval Air Systems Command
AIR 03
Washington, D.C. 20360 2 Copies

Naval Electronic Systems Command
ELEX 03, Room 2046 Munitions Building
Department of the Navy
Washington, D.C. 20360 2 Copies

Director
Naval Research Laboratory
Washington, D.C. 20390
Attn: Code 2027 6 Copies

Commander
U. S. Naval Ordnance Laboratory
Attn: Librarian
White Oak, Md. 21502 2 Copies

Commanding General
Attn: STEWS-RE-L, Technical Library
White Sands Missile Range
New Mexico 88002 2 Copies

Commander
Naval Electronics Laboratory Center
Attn: Library
San Diego, Calif 92152 2 Copies

Raytheon Company
Attn: Librarian
Bedford, Massachusetts 01730

Dr. L. M. Hollingsworth
AFCRL (CRN)
L. G. Hanscom Field
Bedford, Massachusetts 01731

Division of Engineering & Applied Physics
210 Pierce Hall
Harvard University
Cambridge, Massachusetts 02138

Director
Research Laboratory of Electronncs
Massachusetts Institute of Technology
Cambridge, Massachusetts 02139

Materials Center Reading Room 13-2137
Massachusetts Institute of Technology
Cambridge, Mass. 02139

Project MAC
Document Room
Massachusetts Institute of Technology
545 Technology Square
Cambridge, Mass. 02139

Raytheon Company
Research Division Library
28 Seyon St
Waltham, Massachusetts 02154

Sylvania Electronic Systems
Applied Research Laboratory
Attn: Documents Librarian
40 Sylvan Road
Waltham, Mass. 02154

Commanding Officer
Army Materials & Mechanics Res. Center
Attn: Dr. H. Priest
Watertown Arsenal
Watertown, Mass. 02172

Lincoln Laboratory
Massachusetts Institute of Technology
Lexington, Massachusetts 02173

Commanding Officer
Office of Naval Research Branch Office
495 Summer Street
Boston, Massachusetts 02210

Commanding Officer (Code 2064)
Navy Underwater Sound Laboratory
Fort Trumbull
New London, Connecticut 06320

Yale University
Engineering Department
New Haven, Connecticut 06520

Commanding General
U. S. Army Electronics Command
Attn: AMSEL-HL-CT-A
Fort Monmouth, New Jersey 07703

Commanding General
U. S. Army Electronics Command
Attn: AMSEL-HL-CT-DD
Fort Monmouth, New Jersey 07703

Commanding General
U. S. Army Electronics Command
Attn: AMSEL-HL-CT-I
Fort Monmouth, New Jersey 07703

Commanding General
U. S. Army Electronics Command
Attn: AMSEL-HL-CT-L (Dr W. S. McAfee)
Fort Monmouth, New Jersey 07703

Commanding General
U. S. Army Electronics Command
Attn: AMSEL-HL-CT-O
Fort Monmouth, New Jersey 07703

Commanding General
U. S. Army Electronics Command
Attn: AMSEL-HL-CT-R
Fort Monmouth, New Jersey 07703

Commanding General
U. S. Army Electronics Command
Attn: AMSEL-KL-D
Fort Monmouth, New Jersey 07703

Commanding General
U. S. Army Electronics Command
Attn: AMSEL-KL-E
Fort Monmouth, New Jersey 07703

Commanding General
U. S. Army Electronics Command
Attn: AMSEL-KL-M (Drs Schie./Hieslmair)
Fort Monmouth, New Jersey 07703

Commanding General
U. S. Army Electronics Command
Attn: AMSEL-KL-S (Dr. H. Jacobs)
Fort Monmouth, New Jersey 07703

Commanding General
U. S. Army Electronics Command
Attn: AMSEL-KL-T
Fort Monmouth, New Jersey 07703

Commanding General
U. S. Army Electronics Command
Attn: AMSEL-NL-A
Fort Monmouth, New Jersey 07703

Commanding General
U. S. Army Electronics Command
Attn: AMSEL-NL-D
Fort Monmouth, New Jersey 07703

Commanding General
U. S. Army Electronics Command
Attn: AMSEL-NL-P-2 (Dr. Haratz)
Fort Monmouth, New Jersey 07703

Commanding General
U. S. Army Electronics Command
Attn: AMSEL- NL-P
Fort Monmouth, New Jersey 07703

Commanding General
U. S. Army Electronics Command
Attn: AMSEL-NL-R (Mr. R. Kulnyi)
Fort Monmouth, New Jersey 07703

Commanding General
U. S. Army Electronics Command
Attn: AMSEL-NL-S
Fort Monouth, New Jersey 07703

Commanding General
U. S. Army Electronics Command
Attn: AMSEL-RD-GF
Fort Monmouth, New Jersey 07703

Commanding General
U. S. Army Electronics Command
Attn: AMSEL-RD-MT
Fort Monmouth, New Jersey 07703

Commanding General
U. S. Army Electronics Command
Attn: AMSEL-SC
Fort Monmouth, New Jersey 07703

Commanding General
U.S. Army Electronics Command
Attn: AMSEL-VI-F (R. J. Niemela)
Fort Monmouth, New Jersey 07703

Commanding General
U. S. Army Electronics Command
Attn: AMSEL-VL-D
Fort Monmouth, New Jersey 07703

Commanding General
U. S. Army Electronics Command
Attn: AMSEL-WL-D
Fort Monmouth, New Jersey 07703

Commanding General
U. S. Army Electronics Command
Attn: AMSEL-XL-C
Fort Monmouth, New Jersey 07703

Commanding General
U. S. Army Electronics Command
Attn: AMSEL-XL-D (Dr. K. Schwidta)
Fort Monmouth, New Jersey 07703

Commanding General
U. S. Army Electronics Command
Attn: AMSEL-XL-E
Fort Monmouth, New Jersey 07703

Commanding General
U. S. Army Electronics Command
Attn: AMSEL-XL-S (Dr. R. Buser)
Fort Mouth, New Jersey 07703

Mr. Norman J. Field, AMSEL-RD-S
Chief, Office of Science & Technology
Research and Development Directorate
U. S. Army Electronics Command
Fort Monmouth, New Jersey 07703

Mr. Robert O. Parker, AMSEL-RD-S
Executive Secretary, JSTAC
U. S. Army Electronics Command
Fort Monmouth, New Jersey 07703

Project Manager
Common Positioning & Navigation Systems
Attn: Harold H. Bahr (AMCPM-NS-TM), Bldg.439
U. S. Army Electronics Command
Fort Monmouth, New Jersey 07703

U. S. Army Munitions Command
Attn: Science & Technology Br. Bldg 59
Picatinny Arsenal, SMUPA-VA6
Dover, New Jersey 07801

N. J. A. Sloane
Bell Telephone Laboratories
Mountain Avenue
Murray Hill, New Jersey 07974

European Office of Aerospace Research
APO New York 09667

New York University
College of Engineering
New York, N. Y. 10019

Director
Columbia Radiation Laboratory
Columbia University
538 West 120th St.
New York, N. Y. 10027

Airborne Instruments Laboratory
Deer Park, New York 11729

Mr. Jerome Fox, Research Coordinator
Polytechnic Institute of Brooklyn
333 Jay St.
Brooklyn, N. Y. 11201

Syracuse University
Dept. of Electrical Engineering
Syracuse, N. Y. 13210

Rome Air Development Center
Attn: Documents Library (EMTLD)
Griffiss Air Force Base, N. Y. 13440

Mr. H. E. Webb (EMMIIS)
Rome Air Development Center
Griffiss Air Force Base, N. Y. 13440

Professor James A. Cadzow
Department of Electrical Engineering
State University of New York at Buffalo
Buffalo, N. Y. 14214

Carnegie Institute of Technology
Electrical Engineering Department
Pittsburgh, Pa. 15213

Hunt Library
Carnegie-Mellon University
Schenley Park
Pittsburgh, Pa. 15213

Lehigh University
Dept of Electrical Engineering
Bethelehem, Pennsylvania 18015

Commander (ADL)
Naval Air Development Center
Johnsville, Warminster, Pa. 18974

Technical Director (SMUFA-A2000-107-1)
Frankford Arsenal
Philadelphia, Pennsylvania 19137

Philco Ford Corporation
Communications & Electronics Div.
Union Meeting and Jolly Rods
Blue Bell, Pennsylvania 19422

Director
Walter Reed Army Institute of Research
Walter Reed Army Medical Center
Washington, D.C. 20012

Mr. M. Zane Thornton, Chief, Network Engineering, Communications & Operations Branch, Lister Hill
National Center/Biomedical Communications
8600 Rockville Pike
Bethesda, Maryland 20014

Director
Advanced Research Projects Agency
Department of Defense
Washington, D.C. 20301

Director for Materials Sciences
Advanced Research Projects Agency
Department of Defense
Washington, D.C. 20301

Distribution List, Continued

Dr. A. A. Dougal
Asst. Director (Research)
Ofc. of Defense Res. & Eng.
Department of Defense
Washington, D.C. 20301

Office of Deputy Director
(Research & Information, Rm 3D1037)
Department of Defense
The Pentagon
Washington, D. C. 20301

Headquarters
Defense Communications Agency (340)
Washington, D. C. 20305

Commanding General
U. S. Army Material Command
Attn: AMCRD-TP
Washington, D.C. 20315

Director, U. S. Army Material
Concepts Agency
Washington, D. C. 20315

AFSC (SCTSE)
Andrews Air Force Base, Maryland 20331

Hq USAF (AFRDD)
The Pentagon
Washington, D. C. 20330

Hq USAF (AFRDDG)
The Pentagon
Washington, D. C. 20330

Hq USAF (AFRDSD)
The Pentagon
Washington, D.C. 20330

Dr. I. R. Mirman
AFSC (SCT)
Andrews AFB, Maryland 20331

Naval Ship Systems Command
Ship 031
Washington, D. C. 20360

Naval Ship System Command
Ship 035
Washington, D. C. 20360

Commander
U. S. Naval Security Group Command
Attn: G43
3801 Nebraska Avenue
Washington, D. C. 20390

Director
Naval Research Laboratory
Washington, D. C. 20390
Attn: Dr. A. Brodizinsky, Sup. Elec Div

Director
Naval Research Laboratory
Washington, D. C. 20390
Attn: Dr. W. C. Hall, Code 7000

Director
Naval Research Laboratory
Attn: Library, Code 2029 (ONRL)
Washington, D. C. 20390

Dr. G. M. R. Winkler
Director, Time Service Division
U. S. Naval Observatory
Washington, D. C. 20390

U. S. Post Office Department
Library - Room 1012
12th & Pennsylvania., N. W.
Washington, D. C. 20260

Colonel E. P. Gaines, Jr.
ACDA/FO
1901 Pennsylvania Ave. N. W.
Washington, D. C. 20451

Commanding Officer
Harry Diamond Laboratories
Attn: Mr. Berthold Altman (AMXDO-TI)
Connecticut Ave. & Van Ness St., N.W.
Washington, D.C. 20438

Central Intelligence Agency
Attn: OCR/DD Publications
Washington, D. C. 20505

Dr. H. Harrison, Code RRE
Chief, Electrophysics Branch
National Aeronautics & Space Admin.
Washington, D.C. 20546

Federal Aviation Administration
Attn: Admin Stds Div (MS-110)
800 Independence Ave. S.W.
Washington, D. C. 20590

Director
Nation Security Agency
Attn: TDL
Fort George G. Meade, Md. 20755

The John Hopkins University
Applied Physics Laboratory
Attn: Document Librarian
8621 Georgia Avenue
Silver Springs, Maryland 20910

Commanding Officer
Human Engineering Laboratories
Aberdeen Proving Ground
Aberdeen, Maryland 21005

Commanding Officer (AMXRD-BAT)
U. S. Army Ballistics Research
Laboratory
Aberdeen Proving Ground
Aberdeen, Maryland 21005

Electromagnetic Compatibility
Analysis Center
(ECAC), Attn: ACLP
North Severn
Annapolis, Maryland 21402

Director
U. S. Army Engineer Geodesy
Intelligence & Mapping
Research & Development Agency
Fort Belvoir, Virginia 22060

Dr. G. M. Janney, AMSEL-HL-NVOR
Night Vision Laboratory, USAECOM
Fort Belvoir, Virginia 22060

Dr. A. D. Schnitzler, AMSEL-HL-NVII
Night Vision Laboratory, USAECOM
Fort Belvoir, Virginia 22060

U. S. Army Mobility Equipment Research
and Development Center
Attn: Technical Document Center
Bldg. 315
Fort Belvoir, Virginia 22060

Weapons Systems Evaluation Group
Attn: Colonel Blaine O. Vogt
400 Army-Navy Drive
Arlington, Virginia 22202

Head, Technical Services Division
Naval Investigative Service Headquarters
4420 North Fairfax Drive
Arlington, Virginia 22203

Physical & Engineering Sciences Division
U. S. Army Research Office
3045 Columbia Pike
Arlington, Va. 22204

Lt. Col. H. W. Jackson
Chief, Electronics Division
Directorate of Engineering Sciences
Air Force Office of Scientific Research
Arlington, Virginia 22209

Commanding General
U. S. Army Security Agency
Attn: IARD-T
Arlington Hall Station
Arlington, Virginia 22212

VELA Seismological Center
300 North Washington Street
Alexandria, Virginia 22314

U. S. Naval Weapons Laboratory
Dahlgren, Virginia 22448

Research Laboratories for the Eng.
Sciences, School of Engineering &
Applied Science
University of Virginia
Charlottesville, Va. 22903

Dr. Herman Robl
Deputy Chief Scientist
U. S. Army Research Office (Durham)
Box CM, Duke Station
Durham, North Carolina 27706

Richard O. Ulsh (CRDARD-IPO)
U. S. Army Research Office (Durham)
Box CM, Duke Station
Durham, North Carolina 27706

ADTC (ADBPS-12)
Eglin AFB, Florida 32542

Commanding Officer
Naval Training Device Center
Orlando, Florida 32813

Technical Library, AFETR
(ETV,MU-135)
Patrick AFB, Florida 32935

Commanding General
U. S. Army Missile Command
Attn: AMSMI-REX
Redstone Arsenal, Alabama 35809

Redstone Scientific Information Center
Attn: Chief, Document Section
U. S. Army Missile Command
Redstone Arsenal, Alabama 25809

AUL3T-9663
Maxwell AFB, Alabama 36112

Hq AEDC (AETS)
Attn: Library/Documents
Arnold AFS, Tennessee 37389

Case Institute of Technology
Engineering Division
University Circle
Cleveland, Ohio 44106

NASA Lewis Research Center
Attn: Library
21000 Brookpark Road
Cleveland, Ohio 44135

Professor J. J. D'Azzo
Dept. of Electrical Engineering
Air Force Institute of Technology
Wright-Patterson AFB, Ohio 54533

Director
Air Force Avionics Laboratory
Wright-Patterson AFB, Ohio 45433

AFAL (AVT) Dr H. V. Noble
Electronics Technology Division
Air Force Avionics Laboratory
Wright-Patterson AFB, 45433

AFAL (AVTA) R. D. Larson
Wright-Patterson AFB, Ohio 45433

Dr. Robert E. Fontana
Systems Research Laboratories Inc.
7001 Indian Ripple Road
Dayton, Ohio 45440

Dept. of Electrical Engineering
College of Engineering & Technology
Ohio University
Athens, Ohio 45701

Commanding Officer
Naval Avionics Facility
Indianapolis, Indiana 46241

Dr. John D. Hancock, Head
School of Electrical Engineering
Purdue University
Lafayette, Ind 47907

Professor Joseph E. Rowe
Chairman, Dept of Electrical
Engineering
The University of Michigan
Ann Arbor, Michigan 48104

Dr. G. J. Murphy
The Technological Institute
Northwestern University
Evanston, Ill. 60201

Commanding Officer
Office of Naval Research Branch Office
219 South Dearborn St.
Chicago, Illinois 60604

Illinois Institute of Technology
Dept. of Electrical Engineering
Chicago, Ill 60616

The University of Arizona
Dept. of Electrical Engineering
Tucson, Ariz. 85721

Commander Test Command (TCDT-)
Defense Atomic Support Agency
Sandia Base
Albuquerque, N. M. 87115

Los Alamos Scientific Laboratory
Attn: Report Library
P. O. Box 1663
Los Alamos, N. M. 87544

Atmospheric Sciences Office
Atmospheric Sciences Laboratory
White Sands Missile Range
New Mexico 88002

Commanding Officer
U. S. Army Electronics R & D Activity
White Sands Missile Range
New Mexico 88002

Missile Electronic Warfare
Technical Area, AMSEL-WT-MT
White Sands Missile Range
New Mexico 88002

Director
Electronic Sciences Lab.
University of Southern California
Los Angeles, Calif. 90007

Engineering & Mathematical Sciences
Library
University of California at Los Angeles
405 Hilgred Avenue
Los Angeles, Calif. 90024

Aerospace Corporation
P.O. Box 95085
Los Angeles, California 90045
Attn: Library Acquisitions Group

Det 6, Hq OAR
Air Force Unit Post Office
Los Angeles, Calif. 90045

Director, USAF PROJECT RAND
Via: Air Force Liaison Office
The RAND Corporation
Attn: Library D
1700 Main Street
Santa Monica, California 90045

Hq SAMSO (SMTTA)Lt Nelson
AF Unit Post Office
Los Angeles, Calif. 90045

Dr. Sheldon J. Wells
Electronic Properties Information Center
Mail Station E-175
Hughes Aircraft Company
Culver City, California 90230

Director
Coordinated Science Laboratory
University of Illinois
Urbana, Illinois 61801

Commandant
U. S. Army Command & General Staff
College
Attn: Acquisitions, Library Division
Fort Leavenworth, Kansas 66027

Dept of Electrical Engineering
Rice University
Houston, Texas 77001

HQ AMD (AMR)
Brooks AFB, Texas 78235

USAFSAM (SMKOR)
Brooks AFB, Texas 78235

Mr B. R. Locke
Technical Advisor, Requirements
USAF Security Service
Kelly Air Force Base, Texas 78241

Director
Electronics Research Center
The University of Texas at Austin
Austin, Texas 78712

Department of Electrical Engineering
Texas Technological College
Lubbock, Texas 79409

Commandant
U. S. Army Air Defense School
Attn: Missile Sciences Div., C&S Dept.
P.O. Box 9390
Fort Bliss, Texas 79916

Director
Aerospace Mechanics Division
Frank J. Seiler Research Laboratory (OAR)
USAF Academy
Colorado Springs, Colorado 80840

Director of Faculty Research
Department of the Air Force
U. S. Air Force Academy
Colorado Springs, Colorado 80840

Academy Library (DFSLB)
U. S. Air Force Academy
Colorado Springs, Colorado 80912

Utah State University
Dept of Electrical Engineering
Logan, Utah 84321

School of Engineering Sciences
Arizona State University
Tempe, Ariz. 85281

Commanding General
U. S. Army Strategic Communications
Command
Attn: SCC-CG-SAE
Fort Huachuca, Arizona 85613

Deputy Director and Chief Scientist
Office of Naval Research Branch Office
1030 East Green Street
Pasadena, California 91101

Aeronautics Library
Graduate Aeronautical Laboratories
California Institute of Technology
1201 E. California Blvd.
Pasadena, California 91109

Professor Nicholas George
California Inst. of Technology
Pasadena, California 91109

Commanding Officer
Naval Weapons Center
Corona Laboratories
Attn: Library
Corona, California 91720

Hollander Associates
P.O. Box 2276
Fullerton, California 92633

Commander, U.S. Naval Missile Center
Point Mugu, California 93041

W. A. Eberspacher, Associate Head
Systems Integration Division
Code 5340A, Box 15
U. S. Naval Missile Center
Point Mugu, California 93041

The Library
Government Publications Section
University of California
Santa Barbara, California 93106

Commander (Code 753)
Naval Weapons Center
Attn: Technical Library
China Lake, California 93555

Library (Code 2124)
Technical Report Section
Naval Postgraduate School
Monterey, California 93940

Glen A. Myers (Code 52Mv)
Assoc Professor of Elec. Engineering
Naval Postgraduate School
Monterey, California 93940

Dr. Leo Young
Stanford Research Institute
Menlo Park, California 94025

Union Carbide Corporation
Electronic Division
P.O. Box 1209
Mountain View, California 94041

Lenkurt Electric Co., Inc.
1105 County Road
San Carlos, California 94070
Attn: Mr. E. K. Peterson

Director
Microwave Physics Laboratory
Stanford University
Stanford, California 94305

Director
Stanford Electronics Laboratories
Stanford University
Stanford, California 94305

Nuclear Instrumentation Group
Bldg 29, Room 101
Lawrence Radiation Laboratory
University of California
Berkeley, California 94720

Director, Electronics Research
Laboratory
University of California
Berkeley, California 94720

Security Classification

DOCUMENT CONTROL DATA - R & D

(Security classification of title, body of abstract and indexing annotation must be entered when the overall report is classified)

1. ORIGINATING ACTIVITY *(Corporate author)*	2a. REPORT SECURITY CLASSIFICATION
University of Illinois Coordinated Science Laboratory Urbana, Illinois 61801	2b. GROUP

3. REPORT TITLE

TUNNELING SPECTROSCOPY IN DEGENERATE p-TYPE SILICON

4. DESCRIPTIVE NOTES *(Type of report and inclusive dates)*

5. AUTHOR(S) *(First name, middle initial, last name)*

CULLEN, D.E., WOLF E.L., COMPTON W. DALE

6. REPORT DATE	7a. TOTAL NO. OF PAGES	7b. NO. OF REFS
February, 1970	45	32

8a. CONTRACT OR GRANT NO.	9a. ORIGINATOR'S REPORT NUMBER(S)
DAAB 07-67-C-0199; also in part Jet	
b. PROJECT NO. Propulsion Laboratory Contract No. 952383	R-457
c.	9b. OTHER REPORT NO(S) *(Any other numbers that may be assigned this report)* UILU -ENG 70-202
d.	

10. DISTRIBUTION STATEMENT

This document has been approved for public release and sale; its distribution is unlimited.

11. SUPPLEMENTARY NOTES	12. SPONSORING MILITARY ACTIVITY
	Joint Services Electronics Program thru U.S. Army Electronics Command Fort Monmouth, New Jersey 07703

13. ABSTRACT

Tunneling in boron doped p-type silicon metal-semiconductor (MS) and metal-insulator-semiconductor (MIS) tunnel junctions has been studied at low temperatures by measuring the derivatives, dI/dV and d^2I/dV^2, of the current-voltage characteristics as functions of applied bias voltage V. The boron impurity concentration of the silicon crystals varied from 6.5×10^{18} cm^{-3} to 2.3×10^{20} cm^{-3}. Junctions were prepared by evaporating metal contacts onto vacuum or air cleaved silicon surfaces.

The general features of the tunneling conductance were found to be in qualitative agreement with existing theories of tunneling in semiconductors. Structure in the derivative data resulting from the interaction of tunneling electrons with silicon zone center phonons and boron local mode phonons has been observed. The optical phonon lineshapes in the most heavily doped MIS units are shown to compare well with the theoretical lineshapes in which modifications in the bulk semiconductor states arising from electron-optical phonon interactions in the semiconductor electrode have been included. The origin of the optical phonon and local mode phonon structure in samples of lower doping is not fully understood.

DD FORM 1 NOV 65 1473

Security Classification

Security Classification

14 KEY WORDS	LINK A		LINK B		LINK C	
	ROLE	WT	ROLE	WT	ROLE	WT
Metal-semiconductor Tunneling						
Electron-Phonon Interactions						

Security Classification